University of Oxford

MSc in Mathematical Modelling and Scientific Computing

Dissertation

Solitary wave propagation across interfaces in 1D granular crystals

Armin Kekić
St Hugh's College

Trinity 2016

Dedication

Mojoj mami.

Acknowledgements

I thank Dr Robert Van Gorder for his supervision for this dissertation and many helpful suggestions and fruitful discussions. I am grateful for the continuous support by Dr Kathryn Gillow throughout the course. Last, but by no means least, I would like to thank the MMSC class for the comradery, enthusiasm and numerous competitions at the foosball table in the last year.

Abstract

In this dissertation we present a numerical study of solitary wave propagation in 1D granular crystals with Hertz-like interaction potentials. We consider interfaces between media with different exponents in the interaction potential. For an interface with increasing interaction potential exponent along the propagation direction we obtain mainly transmission with delayed secondary transmitted and reflected pulses. For interfaces with decreasing interaction potential exponent we observe both significant reflection and transmission of the solitary wave, where the transmitted part of the wave forms a multipulse structure. We investigate impurities consisting of beads with different interaction exponents compared to the medium they are embedded in. We find that the impurities cause both reflection and transmission, including the formation of a multipulse structure, independently of whether the exponent in the impurities is smaller or larger than in the embedding medium. For wave propagation effects at interfaces and impurities we give an explanation in terms of quasi-particle collisions. Lastly, we study disorder and periodicity in the interaction potential exponents. Solitary waves in media with randomised interaction exponents experience exponential decay, where the dependence of the decay rate is similar to the case of randomised bead masses. For chains with interaction exponents alternating between two values we find qualitatively different propagation properties depending on the choice of the two exponents. We find regimes with exponential decay and stable solitary wave propagation with pairwise collective behaviour. For certain exponent values we observe a new type of stable confined wave, with a periodically changing wave form.

Contents

1 Introduction

Granular materials are composed of a large number of discrete, solid macroscopic particles such as sand, rice or snow; and they play an important role in many aspects of industry and science such as construction, agriculture or geological processes. They are often viewed as a fourth state of matter as they can exhibit characteristics of gases, liquids or solids, depending on the circumstances [2].

Figure 1.1: Newton's cradle. Source: [1].

In this thesis we consider ordered granular materials, so-called *granular crystals*. In one dimension these consist of a linearly aligned chain of particles, whereas in higher dimensions the specific packing of the grains can play a role in the ordering [3]. One example of a granular crystal the reader might be familiar with is Newton's cradle, as shown in Figure 1.1. Upon pulling one ball away and letting it fall back onto the array, the ball on the opposite end is pushed off, seemingly without any effect on the intermediate balls. The ejected ball then swings back onto the array, repeating the motion from the other side. While this appears to be merely an interesting demonstration of basic Newtonian mechanics [4], systems similar to Newton's cradle can facilitate complex dynamics and have spawned serious research from material scientists and applied mathematicians alike [5–13].

One of the most exciting features of granular crystals we want to study is the wave propagation. Compression waves can propagate as solitons or sound waves depending on the interaction potential between the beads and the external compression of the chain. In uniform granular crystals solitons can travel over distances that are orders of magnitude larger than the wavelength without experiencing any change in shape due to dispersion [6]. The type of interaction that leads to non-linear solitary waves is the repulsive Hertz-like contact force that depends on the contact geometry and bead material [14].

Even though solitary waves are stable in uniform granular chains [6], they can undergo drastic changes at interfaces between media with different properties [7]. The wave can be partially transmitted or reflected, and even the full disintegration of the wave into so-called multipulse structures is observed [15, 16]. While most of the work done on interfaces so far focusses on media with different bead masses, we use differences in the contact geometry between the beads as an alternative approach to tweak the wave propagation dynamics at interfaces. The shape of the interaction potential depends on the geometry of the contact region, which in turn affects the wave propagation [7]. In this thesis, we study the wave propagation across interfaces between granular crystals with different interaction potentials.

To model the dynamics of granular crystals it is often desirable to obtain a continuum description of the medium in order to treat the chain analytically. However, unlike most problems in fluid dynamics, a recurring challenge in the study of granular materials is that the discreteness of the system is crucial for understanding the behaviour of the material and cannot be neglected. Hence, analytical studies of the wave propagation in granular crystals has been limited to simple cases such as uniform media [6]. Therefore, the main method used to investigate the dynamics at interfaces used in this thesis is the numerical simulation of the full discrete system of beads.

In Chapters 2 and 3 we present the mathematical model used to describe granular crystals and review relevant previous research. In Chapter 4 we summarise the basics of the numerical implementation for the simulations we carry out. Chapter 5 is dedicated to the study of wave propagation in uniform granular chains under different interaction potentials, which lays the basis for understanding the effects arising at interfaces between different media, which are discussed in Chapter 6. Lastly, we investigate the effect of disorder and periodicity in the bead interaction potential in Chapter 7.

The extent of the source code written for the simulations makes the inclusion of the full code in this thesis impractical. Therefore, we have created an online repository containing all of the classes and methods developed in the course of the study (`https://github.com/mvp15/dissertation-MMSC`). Furthermore, the dynamics that will be described here are often complex and not very well represented by snapshots at particular times. In order to provide more vivid illustrations of the processes described here we uploaded videos showing some of simulations to the repository as well. References to files in the repository are denoted by superscripts in capital letters and are listed on page 59.

2 Hertz-like models for 1D granular crystals

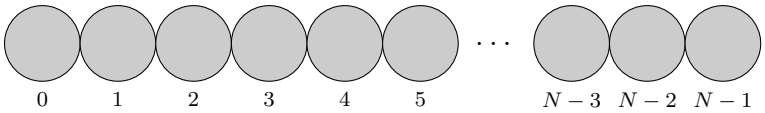

Figure 2.1: Granular chain of spherical beads with contact interaction.

The interesting wave propagation properties in granular crystals, as depicted in Figure 2.1, originate in the interaction between neighbouring beads in the chain. Two elastic bodies in contact experience a repulsive force which depends on the compression. Considering two bodies i and $i+1$ at positions x_i and x_{i+1}, the repulsive force can be obtained by the interaction potential

$$V(\delta_{i,i+1}) = a_{i,i+1}\delta_{i,i+1}^{n_{i,i+1}}, \tag{2.1}$$

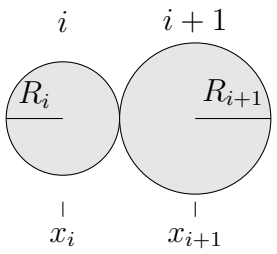

Figure 2.2: Spherical elastic bodies in contact.

where $\delta_{i,i+1}$ is the virtual overlap between the two bodies presuming they would not deform, and $a_{i,i+1}$ is a prefactor depending on the elastic properties of the material and the geometry of the contact region [14, 17]. We assume that the mutual force between beads is given only by contact forces and therefore $V \equiv 0$ for $\delta_{i,i+1} = 0$, *i.e.* there is no long-range interaction. The value of the exponent $n_{i,i+1}$ is determined by the contact region geometry [7, 14].

The repulsive force between beads is related to the interaction potential by

$$F(\delta) = -\frac{\partial}{\partial\delta}V(\delta). \tag{2.2}$$

We only consider interactions with $n_{i,i+1} > 2$, for which the forces between the beads are non-linear in δ. As presented in Chapters 3 and 5, this leads to the formation of non-linear waves, for which the propagation speed depends on the amplitude.

Furthermore, we note that the inter-particle force originating from the potential (2.1) is fully non-linear, *i.e.* the force has no linear component. As a direct consequence of that, sound wave propagation is not possible in granular crystals without external precompression [6]. Such media are sometimes referred to as *sonic vacua*.

For spheres with radii R_i and R_{i+1} the exponent is $n_{i,i+1} = 5/2$ and the prefactor is given by

$$V(\delta_{i,i+1}) \overset{\text{spheres}}{=} \frac{2}{5D_{i,i+1}} \sqrt{\frac{R_i R_{i+1}}{R_i + R_{i+1}}} \delta_{i,i+1}^{5/2}, \quad (2.3)$$

$$D_{i,i+1} = \frac{3}{4} \left[\frac{1-\sigma_i^2}{Y_i} + \frac{1-\sigma_{i+1}^2}{Y_{i+1}} \right], \quad (2.4)$$

where the Young moduli Y_i, Y_{i+1} and the Poisson ratios σ_i, σ_{i+1} are determined by the elastic properties of the bead materials. Equation (2.3) is called *Hertz potential* [18, 19]; systems with the more general interaction potential (2.1) are sometimes called *Hertz-like*.

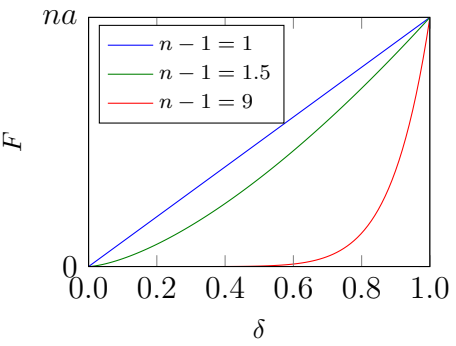

Figure 2.3: Repulsive inter-particle force for different interaction potential exponents n.

The overlap for spherical beads, as shown in Figure 2.2, is given by

$$\delta_{i,i+1} = ((R_i + R_{i+1}) - x_{i+1} + x_i)_+ , \quad (2.5)$$

with $v_+ := \max(v, 0)$. It is often more convenient to write the overlap in terms of the displacements rather than the absolute positions of the beads. For bead i the displacement is $u_i = x_i - x_{i,0}$, where $x_{i,0}$ is the initial position, and the overlap becomes

$$\delta_{i,i+1} = (\Delta_{i,i+1} - u_{i+1} + u_i)_+ . \quad (2.6)$$

The precompression $\Delta_{i,i+1}$ accounts for the fact that the initial position of the beads need not be such that the beads are barely touching, *i.e.* touching but not overlapping. They can also be precompressed by squeezing the chain from both ends.

The potential (2.1) is, strictly speaking, a result for the static case, *i.e.* Equation (2.1) relates the overlap between the beads to an externally applied static force. This result only remains valid for the dynamic case if the time scale of the change in force is much larger than the time that a longitudinal acoustic wave would need to travel across the length of the bead [20]. This restriction ensures that the internal dynamics of the bead can be neglected for the study of the dynamics in the chain. We use

similar chain parameters as in the experimental study carried out by Coste *et.al.* [20] in order ensure the validity of this approximation. Therefore, we can treat the beads as point-like masses that interact via (2.1).

A noteworthy property of the type of granular chains we want to study is that they can be torn apart without any resistance, which is a consequence of the fact that there is no long-range interaction between the beads. This is sometimes referred to as the chain having zero *tensile strength*. Therefore, gaps can open between beads in the chain; and without external compression these can only be closed by interacting with other beads.

From Equation (2.1) one can easily derive Newton's equation of motion for the i^{th} bead, with $i \in \{0, \dots, N-1\}$, in a granular chain

$$\begin{aligned} \frac{\mathrm{d}^2 u_i(t)}{\mathrm{d}t^2} = &+ \frac{n_{i-1,i} a_{i-1,i}}{m_i} \underbrace{(\Delta_{i-1,i} + u_{i-1}(t) - u_i(t))_+^{n_{i-1,i}-1}}_{\text{left neighbour}} \\ &- \frac{n_{i,i+1} a_{i,i+1}}{m_i} \underbrace{(\Delta_{i,i+1} + u_i(t) - u_{i+1}(t))_+^{n_{i,i+1}-1}}_{\text{right neighbour}} \\ &+ \frac{1}{m_i} \underbrace{W_i}_{\text{external field}} . \end{aligned} \tag{2.7}$$

Here, the first two terms describe the interaction with the left and right neighbour respectively. In addition to the mutual repulsive contact force described by Equation (2.1), an external force field, such as gravity, can be applied to the beads, which is accounted for in the last term. For the beads at the end of the chain the relevant neighbour interaction term needs to be set to zero.

Lastly, we define some of the terminology which is be used to describe the dynamics in granular crystals. Chains in which all the beads and precompressions are equal are called *monodisperse*, and *polydisperse* otherwise. We call a bead *excited* if it has significant[1] overlap with at least one of its neighbours; in other words, if there is some potential energy stored in the interaction with a neighbouring bead.

[1] Generally, we use 0.1% of the maximum overlap in the wave as the cut-off value.

3 Previous work

The non-linear interaction potential between beads in granular chains cause them to exhibit interesting wave propagation properties leading to the formation of so-called *solitary waves* [21–23]. First discovered by John Scott Russell in 1834 observing water waves caused by boats in a canal [24], solitary waves are spatially localised "waves of translation". This name arises from the fact that water mass is dragged along with the wave [24]. Other types of waves often disperse, whereas solitary waves are stable over long travelling distances. Building up on the notion of solitary waves, *solitons* are quasi-particles which Drazin and Johnson define to have the following properties [25]:

1. They have a permanent shape;
2. They are localised in space;
3. They remain unchanged by collisions with other solitons, except for a change in phase.

Furthermore, in contrast to linear media, waves in granular crystals are non-linear, *i.e.* the wave speed depends on the amplitude.

There are a number of continuous systems which allow for solitary wave solutions. The Korteweg-de Vries equation (KdV equation)

$$v_t + v_{xxx} - 6vv_x = 0 \tag{3.1}$$

describes waves in shallow water, where $v(x,t)$ is the height of the pulse above the mean water surface level [26]. Other continuous systems giving solitary wave solutions are the non-linear Schrödinger equation [27], describing Bose-Einstein condensates [28], and the sine-Gordon equation [25]. Toda lattices, used to model crystals in solid state physics, are an example for discrete systems with solitary wave solutions. The equation of motion at each lattice site i is given by

$$m_i \frac{\mathrm{d}^2 q_i(t)}{\mathrm{d}t^2} = \mathrm{e}^{-(q_i(t)-q_{i-1}(t))} - \mathrm{e}^{-(q_{i+1}(t)-q_i(t))}, \tag{3.2}$$

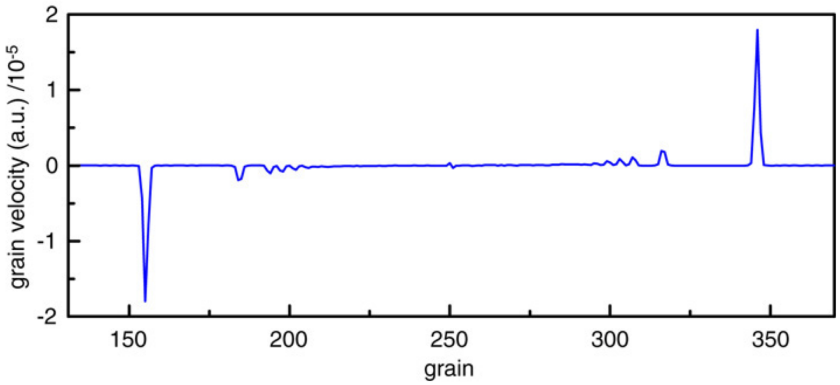

Figure 3.1: Snapshot of two solitary waves after passing each other at grain 250. The trailing solitary waves are smaller waves which emerge from the collision, showing that solitary waves do not remain unchanged by collisions. This image is taken from [7].

where m_i and q_i are the particle mass and displacement, respectively. Toda lattices are similar to the granular crystals studied here, with the primary difference being the exponential interaction potential [29].

The existence of solitary waves in granular chains was first theoretically predicted using a continuum model by Nesterenko [30] and experimentally verified by Lazardi and Nesternko [31] and later by Coste *et.al.* [20]. In the following we will use the terms solitary wave and soliton interchangeably, with the understanding that the waves are solitary waves in terms of the rigorous mathematical definition.

The analytical formulation for the propagation of a single solitary wave through a granular crystal under the assumption of a continuous medium [6, 7] shows good agreement with experiments and numerical simulations for simple solitary wave propagation in monodisperse media [20, 31, 32]. However, in more complex situations the discreteness of granular media can play an essential role for the wave propagation behaviour. For example, in the case of two colliding solitary waves the analytical description predicts that the two waves pass each other without changing their shape and amplidtude, whereas numerical simulations of the discrete medium suggest the emergence of secondary solitary waves from the collision [7, 33, 34] (*cf.* Figure 3.1).

The simplest form of a polydisperse chain is one which consists of two jointed monodisperse granular chains with different bead masses, as shown in Figure 3.2. The behaviour of a solitary wave propagating across the interface between the two media depends on the side from which the wave initially approaches the interface; *i.e.* we observe qualitatively different effects when considering a wave travelling from left

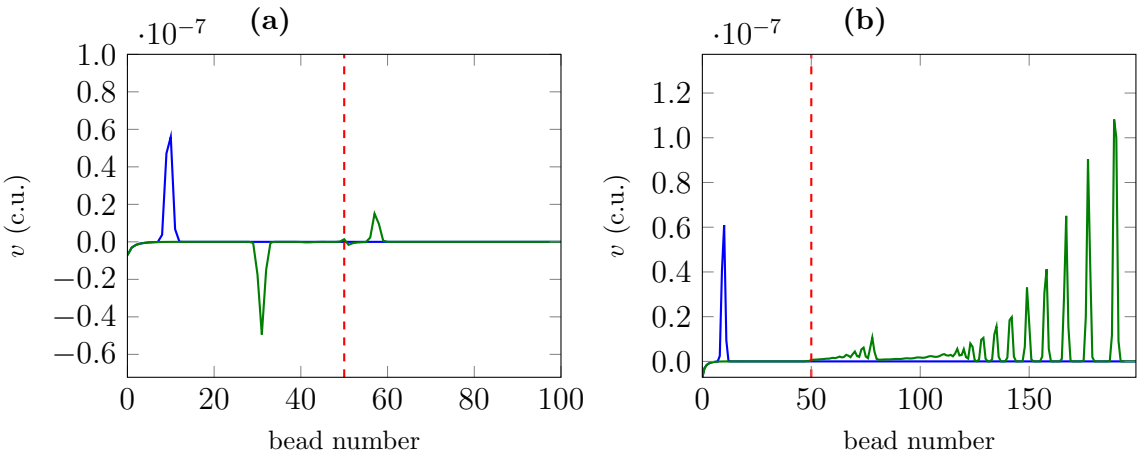

Figure 3.3: Wave propagation across mass interfaces with a ratio of light to heavy mass of 1/8: (a) propagation from light to heavy and (b) from heavy to light. The wave before and after hitting the interface is shown in blue and green respectively. The interface is indicated by the dashed red line.

to right in Figure 3.2, compared to a wave travelling from right to left.

In numerical investigations the partial transmission and reflection of the incoming wave are observed for a solitary wave propagating across an interface from a medium with light grains to one with heavier grains[A]; *i.e.* travelling from left to right in Figure 3.2 [7, 15, 16]. Figure 3.3(a) shows the bead velocities before and after the interaction with the interface. Furthermore, during the splitting of the incoming wave into a transmitted and a reflected part, gaps arise between beads at the vicinity of the interface [16].

Figure 3.2: Chain composed of two media with different bead masses.

Similar effects to those at interfaces between granular crystals with different bead masses have been observed for mass impurities. These impurities are created by changing the mass of a single bead in an otherwise monodisperse granular crystal [7, 32, 35].

For a wave travelling in the opposite direction[B], the incoming wave is fully transmitted and disintegrates forming a multipulse structure [16, 36], as shown in Figure 3.3(b). A second multipulse structure is formed with a delay to the first one. This delay is due to a gap opening and closing between beads at the interface [6].

Wave propagation across mass interfaces is another example in which effects arise as a direct consequence of the discreteness of the medium, as gaps between beads in the vicinity of the interface are crucial for understanding the wave dynamics [6, 16].

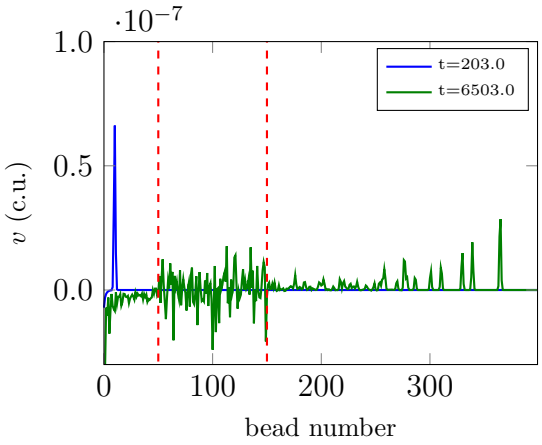

Figure 3.4: Granular container with the mass ratio between the bead masses in the container and the bead masses in the embedding material being 1/8.

These phenomena cannot be captured by the analytical approaches used to describe granular crystals developed so far, due to the assumption of a continuous medium used in such analytical approaches. Consequently, the study of wave propagation across interfaces is limited to numerical simulations.

Granular media have received a lot of attention from material scientists due to their application in the design of impact attenuating materials [5, 9–13]. In order to properly make use of the shock absorbing capabilities of granular crystals, understanding the propagation of solitary waves is indispensable. In granular crystals, designing an impact attenuating material is equivalent to designing a medium that disintegrates or re-directs solitary waves in such a way that the impact of the wave on the area which is to be protected is mitigated.

In 1D, so-called *granular containers* make use of the propagation of waves across mass interfaces in the design of a composite material that is capable of delaying and mitigating the impact of an incoming solitary wave[C]. The simplest form of a granular container is a medium with lighter beads embedded in a medium with heavier beads, as shown in Figure 3.5 [7, 16, 37]. At the first interface a solitary wave disintegrates and forms a multipulse structure inside the container, whereas at the second interface each of these pulses is partially transmitted and reflected. This leads to only a fraction of the initial pulse energy being transmitted after the pulse meets the two interfaces. The remaining energy is held back in the container in the form of several solitary waves which are reflected back forth, losing part of their energy in transmission at each reflection, as shown in Figure 3.4. Thus the impact of the initial solitary wave is attenuated by splitting it into many smaller waves which hit the end of the chain one after the other [16]. This principle of combining interfaces to

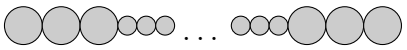

Figure 3.5: Granular container.

manipulate the wave propagation can be further extended to more complex granular container structures [7].

Tapered chains, depicted in Figure 3.6, are chains with slowly increasing bead masses; *i.e.* instead of having one interface with a relatively high difference in bead masses, tapered chains can be seen as a sequence of interfaces. This set-up reflects a fraction of the wave energy at each interface. Tapered chains are characterised by the tapering parameter $q \in (0, 1)$ that relates the radii R_i and R_{i+1} of two successive spherical beads in the tapered part of the chain by $R_{i+1} = (1 - q)R_i$. In numerical simulations it was observed that the wave attenuation is increased with increasing tapering q. The attenuation can be further enhanced in so-called *decorated tapered chains*, where every other bead in the decorated part of the chain is kept at the initial bead size [7, 38].

Figure 3.6: Tapered granular chain.

A similar idea to tapering chains is to introduce disorder in the bead masses. Manciu *et.al.* [7, 39] have studied the effect of randomising the bead masses as

$$m_i = \bar{m}\,(1 + r_i\sigma)\,, \qquad i \in \{0, \ldots, N-1\}, \tag{3.3}$$

with $\bar{m}$ being the mean mass, r_i being a random number that is uniformly distributed in $[-1, 1]$ and σ a parameter weighting the randomness of the masses [7, 39]. This also acts as a sequence of interfaces; however, here the mass difference along the wave propagation can be both positive or negative. For this configuration it was observed that the solitary wave energy E decays as

$$E(x) = E_0 \exp(-\alpha_E x), \tag{3.4}$$

where E_0 is the initial energy and x is the position in the chain. Furthermore, it was found that the decay rate α_E is proportional to σ^2 for small enough σ [7, 39].

Other systems using a sequence of interfaces are granular crystals with alternating bead masses, so-called *dimer* or *di-atomic* granular crystals [40]. However, such systems do not necessarily cause solitary waves to decay. And even though the compression of monodisperse granular chains causes wave dispersion, stable and spatially localised waves could be found for di-atomic chains [41, 42].

4 Numerical method and implementation

For a given chain with N beads Equation (2.7) constitutes a coupled set of N second order non-linear ODEs. Defining the vector of bead displacements as

$$\mathbf{u} = \begin{bmatrix} u_1 \\ u_2 \\ \vdots \\ u_N \end{bmatrix}, \tag{4.1}$$

we can formally write the equation of motion (2.7) as

$$\ddot{\mathbf{u}} = \mathbf{f}(\mathbf{u}), \tag{4.2}$$

where $\ddot{\mathbf{u}}$ denotes the second time derivative of $\mathbf{u}$. By defining the combined vector of bead displacements and velocities

$$\mathbf{z} = \begin{bmatrix} u_1 \\ \vdots \\ u_N \\ v_1 \\ \vdots \\ v_N \end{bmatrix} = \begin{bmatrix} \mathbf{u} \\ \mathbf{v} \end{bmatrix} \qquad \text{where} \qquad \mathbf{v} = \begin{bmatrix} v_1 \\ \vdots \\ v_N \end{bmatrix} = \dot{\mathbf{u}}, \tag{4.3}$$

Equation (4.8) can be converted into a system of 2N first order non-linear ODEs that can be written as

$$\dot{\mathbf{z}} = \mathbf{F}(\mathbf{z}) = \begin{bmatrix} \mathbf{v} \\ \mathbf{f}(\mathbf{u}) \end{bmatrix}. \tag{4.4}$$

The main computational step for simulating the dynamics in granular crystals is solving Equation (4.4), for N of order 10^2 to 10^3.

Implementation in Python

All of the code written for carrying out the simulations and data analysis is written in Python [43], where we mostly use arrays from the Python extension NumPy [44] for data storage. Where applicable, we use the scientific computing library SciPy [45] which has implemented functionality similar to MATLAB.

The main body of the code is organised in two classes: `class Chain`, which encapsulates all the chain properties, and `class Simulation_1D` with the ODE solver and analysis methods. For further details see the code and documentation in the repository[D].

Ghost particles

As mentioned above, the equation of motion for the particles at the boundaries has only one interaction term since it has only one neighbour. In order to avoid having to use separate equations for the boundaries or looping through particles in the ODE solver, we added two ghost particles at the ends of the chain with the interaction prefactor a to the first real particle being zero. Therefore the state vector $\mathbf{z}$ in the simulation becomes

$$\mathbf{z}_{\text{sim}} = \begin{bmatrix} 0 \\ \mathbf{u} \\ 0 \\ \mathbf{v} \end{bmatrix}, \tag{4.5}$$

where there are no extra entries for the velocity of the ghost particle, since they do not move. This way we can write the first order ODE (4.4) solely in terms of Numpy-array objects.

Re-scaling

For typical experimental parameters of the chain [20], the factors scaling like na/m in front of the interaction term in the equation of motion are $\mathcal{O}(10^{12}\,\mathrm{s}^{-2})$ in SI units, since

$$a = \mathcal{O}(10^{9}\,\mathrm{kg\,s}^{-2}), \quad m = \mathcal{O}(10^{-3}\,\mathrm{kg}), \quad n = \mathcal{O}(1). \tag{4.6}$$

In order to scale this factor to $\mathcal{O}(1)$ we re-scale time by

$$t = \beta\tilde{t}, \qquad \beta = \sqrt{\frac{m_0}{\mu n_0}}, \tag{4.7}$$

where μ is the order of magnitude of a such that $\tilde{a} = a/\mu = \mathcal{O}(1\,\mathrm{kg\,s}^{-2})$, and m_0 and n_0 are typical values for the bead mass and interaction potential exponent respectively.

Then the equation of motion after rescaling becomes

$$\begin{aligned}\frac{\mathrm{d}^2 u_i(\tilde{t})}{\mathrm{d}\tilde{t}^2} = &+ \frac{\beta^2 \mu n_{i-1,i}}{m_i} \tilde{a}_{i-1,i} \left(\Delta_{i-1,i} + u_{i-1}(\tilde{t}) - u_i(\tilde{t})\right)_+^{n_{i-1,i}-1} \\ &- \frac{\beta^2 \mu n_{i,i+1}}{m_i} \tilde{a}_{i,i+1} \left(\Delta_{i,i+1} + u_i(\tilde{t}) - u_{i+1}(\tilde{t})\right)_+^{n_{i,i+1}-1} \\ &+ \frac{\beta^2}{m_i} W_i. \end{aligned} \tag{4.8}$$

Note that the corresponding variables in the source code are in the re-scaled version, but are named without tildes or any other extra characters in order to simplify notation.

ODE solver

For solving the ODE system (4.4) we use a solver provided by the built-in ODE interface *scipy.integrate.ode* [46] in the SciPy library. We use the variable-coefficient ODE solver VODE [47–49], which in turn uses Adams-Moulten and backward differentiation methods depending on the stiffness of the system.

Initial conditions

In order to induce waves in the granular chain the initial conditions of the beads are set as

$$u_1, \ldots, u_N = 0, \quad v_1 = v^{(0)}, \quad \text{and} \quad v_2, \ldots v_N = 0, \tag{4.9}$$

which corresponds to the first bead hitting the granular chain from the left and thereby exciting beads in the system, resulting in wave propagation.

The beads are assumed to be made of stainless steel and dimensions are as used in the experimental set-up by Coste *et.al.* in [20]. Furthermore, it is assumed that the distance between the two contact points of the beads is equal to the bead diameter used in [20]. The relevant physical parameters are shown in Table 4.1.

Symbol	Property	Value
R	bead radius	$4\,\mathrm{mm}$
Y	Young's modulus	$2.26 \times 10^{11}\,\mathrm{N\,m^{-2}}$
σ	Poisson's ratio	0.3
ρ	density	$7650\,\mathrm{kg\,m^{-3}}$
m	mass	$2.05\,\mathrm{g}$

Table 4.1: Physical parameters used in simulations [20].

The initial conditions (4.9) are chosen such that the wave speed of the induced solitary wave is in the range of wave speeds experimentally tested in [20]. In computer units, *i.e.* after re-scaling, for spherical beads with masses as in Table 4.1 we set the initial velocity of the left striking bead to be $v^{(0)} = 1 \times 10^7$. The value the initial velocity takes in computer units changes for different re-scaling factors; however in SI units the initial velocities are the same: approximately $0.11\,\mathrm{m\,s^{-1}}$. This initial velocity induces waves with wave speeds that are of the order of waves experimentally measured by Coste *et.al.* [20].

As discussed in Chapter 2, the interaction potential exponent n can be changed experimentally by altering the contact geometry between the beads. However, changing the contact geometry will generally affect the prefactors a as well [14, 19]. For the sake of simplicity, it is assumed that the prefactors are constant over the entire range of exponents tested here. We set the value of the prefactors to the value for spherical beads as in Equations (2.3) and (2.4).

Convergence and error analysis

As there are no analytical solutions of the full discrete ODE system (4.4), there is no direct way to determine the correctness and accuracy of our numerical scheme used for our simulations. However, we can make use of of both previous results and expected physical properties of the system to evaluate the numerical accuracy. The simulations of wave propagation across mass interfaces shown in Figure 3.3 are produced by our numerical scheme and correctly emulate the behaviour in the original publication [15]. Similarly our simulations show good qualitative agreement with results in the literature in the case of randomised bead masses and solitary wave collisions [7, 33].

In order to evaluate the accuracy quantitatively we can make use of the energy conservation in the chain. As there are no dissipative effects built in to the model used to describe the dynamics, we expect all bead-bead collisions to be fully elastic, *i.e.* conserve the total energy. Therefore the energy loss—or gain—qualifies as a measure of the accuracy of the simulation. We use the total kinetic energy

$$E^{\mathrm{kin}} = \sum_{i=0}^{N-1} m_i v_i^2, \tag{4.10}$$

to determine how well the energy is conserved. We define the energy conservation error as

$$\mathrm{error} = \left| \frac{E^{\mathrm{kin}}_{\mathrm{start}} - E^{\mathrm{kin}}_{\mathrm{end}}}{E^{\mathrm{kin}}_{\mathrm{start}}} \right|, \tag{4.11}$$

where $E_{\text{start}}^{\text{kin}}$ and $E_{\text{end}}^{\text{kin}}$ are the total kinetic energies in the chain at the start and the end of the simulation respectively.

Every granular crystal without externally applied forces reaches a steady-state of the bead velocities for long enough simulation times, *i.e.* the beads move at constant velocity with every bead having a smaller velocity than its right-hand-side neighbour. In terms of bead velocities the steady state translates to the bead velocities increasing monotonously with the bead number[1]. In such a situation the total energy in the chain is purely kinetic as the beads are drifting apart without touching each other. Therefore, we measure the kinetic energy at time $t = 0$, before the the striking bead 0 has any overlap with bead 1, and after the chain has reached the steady state. This justifies neglecting the potential energy for calculating the energy conservation error.

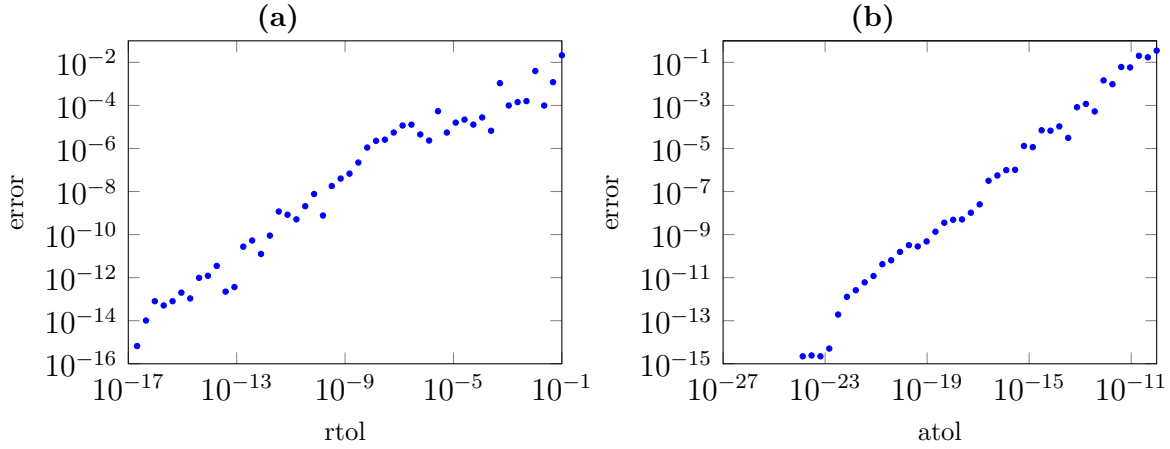

Figure 4.1: Energy conservation error as a function of the relative tolerance (a) and the absolute tolerance (b). For each plot the other tolerance was fixed at 0.0.

In the VODE solver the estimated local error $\mathbf{e}$ is controlled by

$$\left|\frac{e_i}{\text{EWT}_i}\right| \lesssim 1, \qquad i \in \{0, \ldots, N-1\}^2, \tag{4.12}$$

[1] Two subtleties need to be pointed out here: firstly, in order to have purely kinetic energy in the system we additionally need to require the bead overlap to be zero and secondly, for all practical purposes it is enough to require

$$v_{i+1} - v_i > -10^{-5} \times \max_{j \in \{0,\ldots,N-1\}} |v_j|,$$

rather than actual monotonicity. This simplification reduces the simulation time needed to reach the steady state by orders of magnitude, while the additional errors introduced by it are negligible compared to the overall energy conservation error.

[2] Actually we would have to consider the two ghost particles here as well. However, we will neglect

for each component of the error, where the error weights are defined as

$$\mathrm{EWT}_i = \mathrm{rtol} \times |z_i| + \mathrm{atol}, \tag{4.13}$$

where rtol and atol are the relative and absolute tolerances respectively [48, 49].

One can set rtol = 0 or atol = 0 to have a purely absolute tolerance or purely relative tolerance respectively. Figure 4.1 shows the energy conservation error as a function of the two tolerances. We observe that by setting strict tolerances in the simulation the error shrinks to nearly machine precision. This shows that our numerical scheme indeed conserves energy as would be expected from the physical system. In the simulations presented here we choose the tolerances such that the energy conservation error is $\mathcal{O}(10^{-4})$ or smaller. This has shown to be a good trade-off between accuracy and runtime.

them for simpllicity as their position and velocity variables do not change and therefore do not introduce errors.

5 Nonlinear wave propagation in Hertz-like granular crystals

In Chapter 2 a microscopic[1] model in terms of repulsive bead forces is given, explaining the wave propagation in granular chains. A natural question to ask is how these microscopic interactions influence the propagation of waves through the entire system of beads. In this chapter we study the propagation of waves in monodisperse granular chains and how this propagation is affected by changing the interaction potential exponent n.

The known analytical results are recapitulated and compared to our numerical simulations. A numerical study of the wave propagation in monodisperse chains under different interaction exponents n has been carried out by Hascoët *et.al.* [32]; however, understanding the wave propagation in monodisperse chains is essential in order to understand the effects arising in more complex situations such as interfaces in composite media. Therefore, this chapter lays the groundwork for explaining the phenomena presented in later chapters.

Throughout the remainder of this dissertation, we assume all considered media not to be compressed by an external force; hence, $\Delta = 0$ for all beads. Such media are sonic vacua in which no sound wave is possible.

5.1 Analytical results

In the simplest setting of monodisperse granular crystals, the wave propagation through the chain can be described by approximating the the discrete system of beads by a continuous medium. Here we want to revise some of these analytical results, which provide some intuition for the wave propagation dynamics. The following analytical treatment has been developed by Nesterenko and a more detailed discussion can be found in [6, 30, 50, 51].

[1] Here, by microscopic we mean the scale of single beads.

For a monodisperse chain without externally applied precompression, *i.e.* with constant n, a and m over all beads, the equations of motion (2.7) can be written as

$$\ddot{u}_i = A(u_{i-1} - u_i)_+^p - A(u_i - u_{i+1})_+^p, \tag{5.1}$$

where we define $A = na/m$ and $p = n - 1$ in order to simplify the notation. In the following analytical approach the granular chain is regarded as a continuous medium, so that the displacement at bead i can be written as $u_i = u(x,t)$, where x is the spatial coordinate along the chain and t is time. Furthermore, we assume that the typical length scale of the solitary wave L is larger than the bead diameter $\mathfrak{a} = 2R$. This second assumption is also referred to as the *long-wavelength approximation*. The displacement at the neighbouring beads can then be written as an expansion in the small parameter $\varepsilon = \mathfrak{a}/L$, that is

$$u_i = u, \tag{5.2}$$

$$u_{i-1} = u - \mathfrak{a}u_x + \tfrac{\mathfrak{a}^2}{2}u_{xx} - \tfrac{\mathfrak{a}^3}{6}u_{xxx} + \tfrac{\mathfrak{a}^4}{24}u_{xxxx} + \dots\ , \tag{5.3}$$

$$u_{i+1} = u + \mathfrak{a}u_x + \tfrac{\mathfrak{a}^2}{2}u_{xx} + \tfrac{\mathfrak{a}^3}{6}u_{xxx} + \tfrac{\mathfrak{a}^4}{24}u_{xxxx} + \dots\ , \tag{5.4}$$

where we use the shorthand notation $u = u(x,t)$. We can use these expansions to rewrite the displacement differences in (5.1) as

$$u_{i-1} - u_i = \underbrace{-\mathfrak{a}u_x}_{N} \underbrace{+\tfrac{\mathfrak{a}^2}{2}u_{xx} - \tfrac{\mathfrak{a}^3}{6}u_{xxx} + \tfrac{\mathfrak{a}^4}{24}u_{xxxx} + \dots}_{\varphi} = N + \varphi, \tag{5.5}$$

$$u_i - u_{i+1} = \underbrace{-\mathfrak{a}u_x}_{N} \underbrace{-\tfrac{\mathfrak{a}^2}{2}u_{xx} - \tfrac{\mathfrak{a}^3}{6}u_{xxx} - \tfrac{\mathfrak{a}^4}{24}u_{xxxx} + \dots}_{\psi} = N + \psi, \tag{5.6}$$

where N, φ and ψ are functions[2] of x and t. The two terms corresponding to the interaction with the left and respectively right neighbour in the equation of motion become

$$(u_{i-1} - u_i)_+^p \approx (N + \varphi)_+^p, \tag{5.7}$$

$$(u_i - u_{i+1})_+^p \approx (N + \psi)_+^p. \tag{5.8}$$

[2]Note that N in this context is not the same as the number of beads in the chain. We use this notation in order to conform with the notation in [6]

As N and the functions φ and ψ involve terms of different orders in ε it follows that

$$\frac{\varphi}{N} \sim \frac{\psi}{N} \sim \varepsilon, \tag{5.9}$$

which we can use to expand the expressions on the right-hand side of Equations (5.7) and (5.8) as

$$(N+\varphi)_+^p = N^p + pN^{p-1}\varphi + \tfrac{p(p-1)}{2}N^{p-2}\varphi^2 + \tfrac{p(p-1)(p-2)}{6}N^{p-3}\varphi^3 + \dots\ , \tag{5.10}$$

$$(N+\psi)_+^p = N^p + pN^{p-1}\psi + \tfrac{p(p-1)}{2}N^{p-2}\psi^2 + \tfrac{p(p-1)(p-2)}{6}N^{p-3}\psi^3 + \dots\ . \tag{5.11}$$

By plugging these two expansions into (5.1) and re-arranging the terms, the equation of motion for the displacement $u(x,t)$ can now be expressed as a partial differential equation of the form

$$\begin{aligned} u_{tt} = {} & ApN^{p-1}(\varphi-\psi) + A\tfrac{p(p-1)}{2}N^{p-2}\left(\varphi^2-\psi^2\right) \\ & + A\tfrac{p(p-1)(p-2)}{6}N^{p-3}\left(\varphi^3-\psi^3\right) + \dots . \end{aligned} \tag{5.12}$$

Using the definitions of φ and ψ in Equations (5.5) and (5.6), one finds

$$\varphi - \psi = \mathfrak{a}^2 u_{xx} + \tfrac{\mathfrak{a}^4}{12}u_{xxxx} + \mathcal{O}(\varepsilon^6), \tag{5.13}$$

$$\varphi^2 - \psi^2 = -\tfrac{\mathfrak{a}^5}{3}u_{xx}u_{xxx} + \mathcal{O}(\varepsilon^7), \tag{5.14}$$

$$\varphi^3 - \psi^3 = \tfrac{\mathfrak{a}^6}{4}u_{xx}^3 + \mathcal{O}(\varepsilon^7), \tag{5.15}$$

which implies

$$\begin{aligned} u_{tt} = A\mathfrak{a}^{p+1}\Big\{ & p(-u_x)^{p-1}u_{xx} + \tfrac{p}{12}\mathfrak{a}^2(-u_x)^{p-1}u_{xxxx} - \tfrac{p(p-1)}{6}(-u_x)^{p-2}u_{xx}u_{xxx} \\ & + \tfrac{p(p-1)(p-2)}{24}\mathfrak{a}^4(-u_x)^{p-3}u_{xx}^3\Big\} + \mathcal{O}(\varepsilon^3), \end{aligned} \tag{5.16}$$

where $N = -\mathfrak{a}u_x$ was used. The neglected orders in the expansions (5.13)–(5.15) were chosen such that Equation (5.16) includes terms up to $\mathcal{O}(\varepsilon^2)$. From now on we will drop the order of the error, keeping in mind that the equation is only accurate to $\mathcal{O}(\varepsilon^3)$. Equation (5.16) can be written in a more convenient form as

$$u_{tt} = -A\mathfrak{a}^{p+1}\Big\{p(-u_x)^p + \tfrac{p\mathfrak{a}^2}{24}\Big[(p-1)(-u_x)^{p-2}u_{xx}^2 - 2(-u_x)^{p-1}u_{xxx}\Big]\Big\}_x \tag{5.17}$$

for $-u_x > 0$. Defining $\xi = -u_x$ and differentiating in x, this can be written as

$$\xi_{tt} = c_p^2 \Big\{ p\xi^p + \tfrac{p\mathfrak{a}^2}{24} \Big[(p-1)\xi^{p-2}\xi_x^2 + 2\xi^{p-1}\xi_{xx} \Big] \Big\}_{xx}, \tag{5.18}$$

where $c_p^2 = A\mathfrak{a}^{p+1}$. Since solitary waves are translated along the chain without changing the wave form, the solution is expected to be a function of $\tau := x - Vt$, where V is the wave speed of the solitary wave. Using the chain rule

$$\frac{\partial \xi}{\partial x} = \frac{\partial \xi}{\partial \tau}\frac{\partial \tau}{\partial x} = \frac{\partial \xi}{\partial \tau} \quad \text{and} \quad \frac{\partial \xi}{\partial t} = \frac{\partial \xi}{\partial \tau}\frac{\partial \tau}{\partial t} = -V\frac{\partial \xi}{\partial \tau}, \tag{5.19}$$

Equation (5.18) can be expressed as an ordinary differential equation, which upon integrating twice in τ yields

$$\left(\frac{V}{c_p}\right)\xi_{\tau\tau} = \xi^p + \frac{p\mathfrak{a}^2}{24}\left[(p-1)\xi^{p-2}\xi_\tau^2 + 2\xi^{p-1}\xi_{\tau\tau}\right] + \tilde{C}_1\tau + \tilde{C}_0, \tag{5.20}$$

with $\tilde{C}_0$, $\tilde{C}_1$ being integration constants. As ξ needs to stay finite for $\tau \to \pm\infty$, $\tilde{C}_1$ needs to vanish.

Introducing the change of variables

$$y = \xi^{\frac{p+1}{2}}\left(\frac{c_p}{V}\right)^{\frac{p+1}{p-1}}, \qquad \mu = \frac{x}{\mathfrak{a}}\sqrt{\frac{6(p+1)}{p}}, \tag{5.21}$$

(5.20) reduces to the equation of motion for a nonlinear oscillator

$$y_{\mu\mu} = -\frac{\partial W(y)}{\partial y}, \tag{5.22}$$

where W is the oscillator potential field

$$W(y) = \frac{y^2}{2} - \frac{p+1}{4}y^{\frac{4}{p+1}} + Cy^{\frac{2}{p+1}}, \tag{5.23}$$

and C is a free constant arising from the integration constant $\tilde{C}_0$.

One solution of (5.20) is

$$\xi = \left\{\frac{(p+1)}{2}\frac{V^2}{c_p^2}\right\}^{\frac{1}{p-1}}\left|\sin\left(\frac{p-1}{p+1}\sqrt{\frac{6(p+1)}{p}}\frac{\tau}{\mathfrak{a}}\right)\right|^{\frac{2}{p-1}}. \tag{5.24}$$

In terms of $n = p + 1$, Equation (5.24) gives

$$\xi = \underbrace{\left\{ \frac{n}{2} \frac{V^2}{c_{n-1}^2} \right\}^{\frac{1}{n-2}}}_{\xi_{\max}} \left| \sin\left(\underbrace{\frac{n-2}{\mathfrak{a}n} \sqrt{\frac{6n}{n-1}}}_{\omega} \tau \right) \right|^{\frac{2}{n-2}}. \tag{5.25}$$

For solitary waves emerging in granular chains the solutions (5.24) and (5.25) are compactly supported, where the chain has non-zero bead velocity over a span of π/ω, *i.e.* one hump of the sine-term. At the peak of the solitary wave, the sine-term is equal to one and we can solve for the solitary wave velocity to find

$$V = \sqrt{\frac{2c_{n-1}^2}{n}} \xi_{\max}^{\frac{n-2}{2}} = \left(\frac{2c_{n-1}^2}{n} \right)^{\frac{1}{n}} v_{\max}^{\frac{n-2}{n}}, \tag{5.26}$$

where $v_{\max}$ is the maximum bead velocity in the solitary wave. This is in accordance with what we would expect for a non-linear wave as its velocity depends on its amplitude. In the limit $n \to 2$, the right factor containing the solitary wave amplitude goes to 1 and we retrieve the linear wave behaviour with a constant wave velocity.

The typical lengthscale of the solitary wave is determined by the prefactor ω in the sine-term

$$L_n = \frac{\pi \mathfrak{a}}{n-2} \sqrt{\frac{n(n-1)}{6}}. \tag{5.27}$$

Note that L_n stays finite as $n \to \infty$, whereas $V \to 0$.

5.2 Numerical results

Figure 5.1 shows the emergence of a solitary wave in a granular chain of spherical beads[EF]. We observe that within the first 10 beads a stable compression wave of constant shape develops. The solitary wave can be viewed as the balance of two processes: firstly, the compression of a part of the chain caused by the momentum of the initial strike and secondly, the decompression due to the repulsive contact forces. The wave keeps its shape even after travelling over distances which are more than two orders of magnitude larger than its characteristic length. This stability is a typical feature for solitary waves. We numerically simulated chains with lengths of up to 2000 beads and the waves propagating along these chains kept their shape, showing no signs of dispersion. Furthermore the beads in front of and behind the solitary wave are at rest, however the beads behind the wave have been moved forward and are therefore displaced from their initial position.

After the first bead strikes the rest of the chain, note that not all of the energy is converted into the solitary wave. Part of this energy is reflected, causing the first ≈ 5 beads to fly off in the opposite direction. This effect is referred to as *chain fragmentation* and has been observed both in numerical studies [16, 52] and experimentally [6, 36]. Since the rebound velocities decay exponentially with bead number, we can neglect this effect for the wave propagation sufficiently far away from the chain end [52].

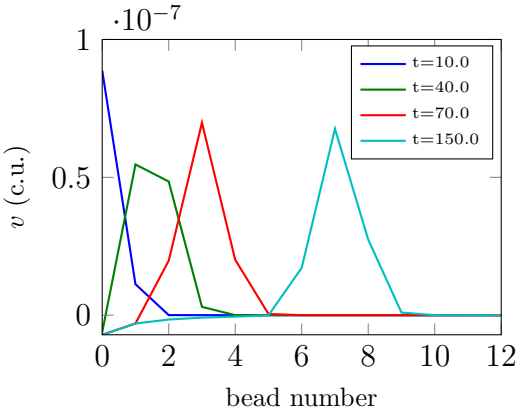

Figure 5.1: Emerging wave in the granular chain after being struck from the left, with $n = 2.5$ and $v^{(0)} = 1\times10^{-7}$. The bead velocities and times are given in computer units.

5.2.1 Wave shape

As we can see from Figure 5.1, at a given point in time there are only a few beads that actually form the solitary wave. However, this makes the investigation of the wave shape challenging as more than a few data points are necessary to make a meaningful analysis. In order to collect more data on the wave shape we use the velocity distribution of the chain at q time steps $t_\alpha \in \{t_1, \ldots, t_q\}$, which we write as v_i^α for the velocity of bead i at time t_α with $i \in \{0, \ldots, N-1\}$. In the continuum model of the chain this can be viewed as evaluating the velocity distribution $v(x,t)$ over a mesh of discrete points in time and space, *i.e.*

$$v(x_i, t_\alpha) = v_i^\alpha, \tag{5.28}$$

where x_i, $i \in \{0, \ldots, N\}$ are the bead positions. Since we expect the bead velocity distribution in the solitary wave v_{sw} to be a function of the travelling-wave variable $\tau = x - Vt$, where V is the speed of the wave, we need to translate the data into the frame of the solitary wave. Therefore we shift the x-position of the distribution to where it would have been at time t_1, *i.e.*

$$v_{\text{sw}}(x_i - Vt_\alpha) = v_i^\alpha. \tag{5.29}$$

Furthermore, since the position of the solitary wave at time t_1 is of no particular interest we shift the x-axis such that the wave maximum is located at $x = 0$.

However, translating the data into the frame of the solitary wave relies on having an accurate estimate of the wave speed V. Measuring the distance the wave travels in the chain for a given time turns out not to be accurate enough, yielding a bad overlap of the data points. In order to make a better choice for V we can make use of what we expect the solitary wave to look like. From the analytical treatment discussed in Section 5.1, we expect the solitary wave to be of the form

$$v_{\mathrm{sw}} = \begin{cases} A\left|\cos\left(B\tau\right)\right|^{\frac{2}{n-2}}, & \text{for } \tau \in \left[-\frac{\pi}{2B}, \frac{\pi}{2B}\right], \\ 0, & \text{otherwise,} \end{cases} \tag{5.30}$$

as shown in Figure 5.2(a). In order to determine the wave speed, we minimise the mean-squared error of the least-squares fit of function given in Equation (5.30) as a function of V. So, at every step of the minimisation we carry out a least-squares fit of (5.30) with A and B as parameters.

The wave shapes for two values of n are shown in Figure 5.3. For small n-values the wave shape in the simulation is described well by the continuum model, whereas the simulated wave deviates significantly from the continuum model prediction for higher values of n. In the derivation of the wave shape in the continuum model we assume that the typical length scale of the solitary wave is much greater than one bead diameter. However, the waves in Figure 5.3(b) span less than two bead diameters. Therefore, the long-wavelength approximation is no longer applicable for large n. Qualitatively the simulation differs most significantly at the edges of the wave, where the continuum model predicts a steeper rise of the bead velocity than what is observed in the simulation. However, the overall extent of the wave appears to be captured well by the continuum model.

The definition of the wavelength of a solitary wave is not obvious. Due to their confinement in space, the period of the wave is technically infinite, which prohibits the standard definition of the wavelength as for periodic waves. Fortunately, the analytically derived wave shape provides a typical length scale of the wave by Equation (5.27), which we will use as the definition of the wavelength. In order to determine the wavelength in the simulation we carry out a least-squares fit of (5.30) and set the wavelength λ to

$$\lambda = \frac{\pi}{B}. \tag{5.31}$$

As the qualitative shape of the model wave shape deviates significantly at the ends of the wave, we only use the middle part of the wave for fitting Equation (5.30). For

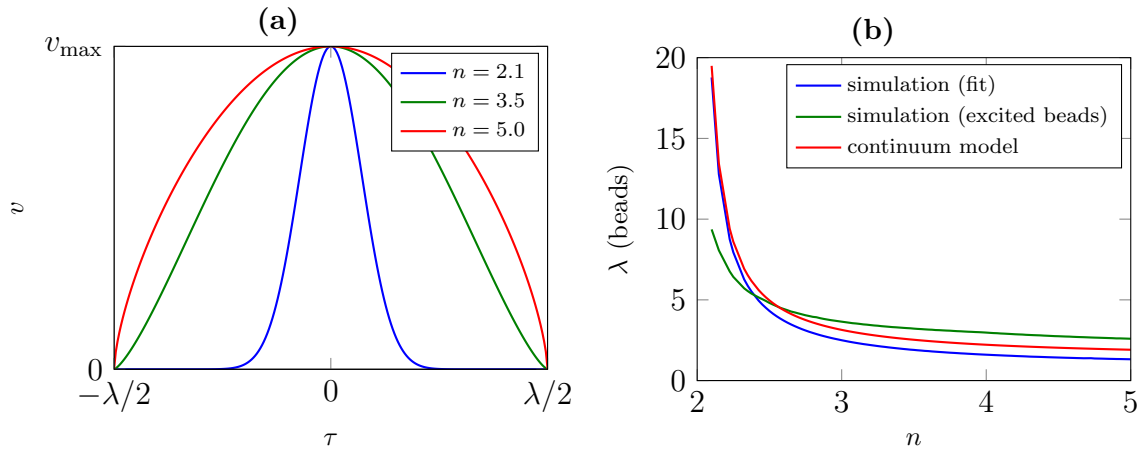

Figure 5.2: Wave shape derived from the continuum model (a) and comparison of wave lengths measured in the simulation and predicted by the continuum model (b).

selecting the fit data we use the half of the wave maximum as a cut-off value below which the data is neglected.

The wave lengths for different n predicted by the model and measured by fitting the wave form (5.30) are shown in Figure 5.2(b). For small n-values, for which the long-wavelength approximation is applicable, the measured wavelengths show good agreement with the model. However, as the wave shape shown in Figure 5.3(b) already suggests, the wave lengths measured by fitting the wave shape are smaller than the model wavelength for large n.

There are two reasons for which one might find the wavelength definition given in (5.31) misleading or inaccurate. First, for small values of n, the length of the chain for which the beads have a significant velocity compared to the peak velocity is clearly smaller than the nominal wavelength, as shown in Figure 5.2(a). On the other hand, the wave shape neglects the tails of the wave, which have significant bead velocities for larger n. One could alternatively define the wavelength as the number of excited particles, *i.e.* the number of beads with more than, say, 0.1% of the peak bead overlap. The wavelength according to this alternative definition is also plotted in Figure 5.2(b). As expected, the wavelength in this alternative definition is smaller than the model wavelength for small n, and greater for larger n. In any case, the wavelength is bounded from below and converges to the lower bound as $n \to \infty$.

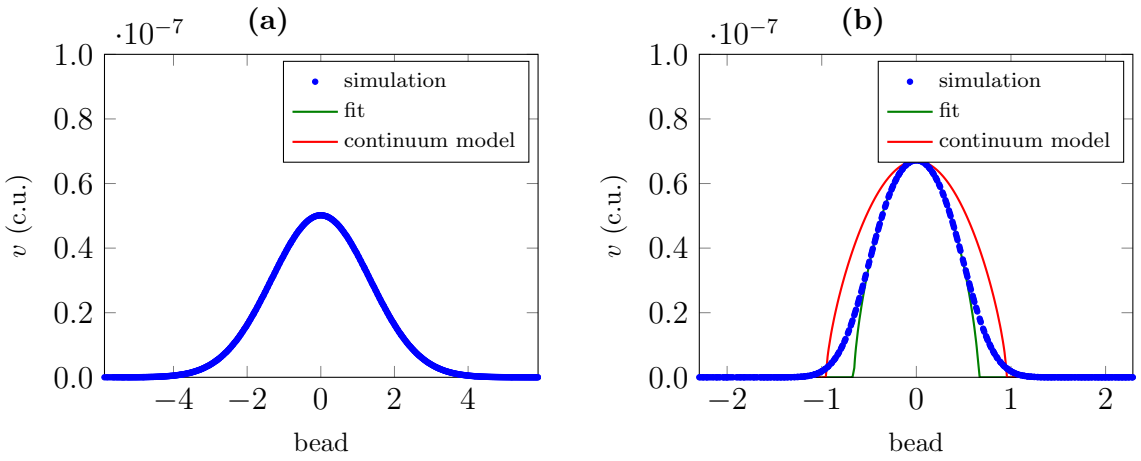

Figure 5.3: Comparison of the wave shape between the prediction from the continuum model and the simulation for $n = 2.1$ (a) and $n = 5.0$ (b).

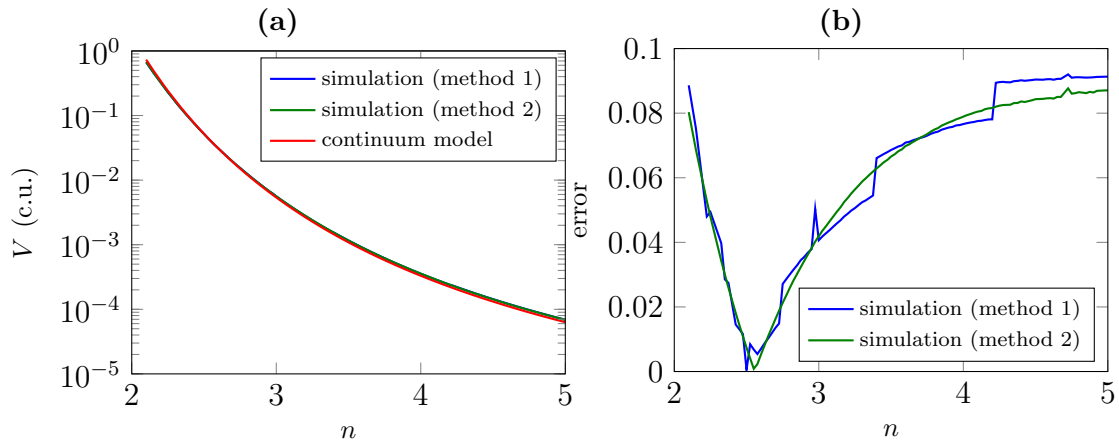

Figure 5.4: Wave speeds for different interaction potential exponents n (a), and the absolute relative error to the continuum model (b).

5.2.2 Wave speed

The wave speed of the solitary wave can be measured by determining the distance the peak of maximum bead velocity has travelled in a given period of time. The wave speed for different values of the interaction potential exponent n is shown in Figure 5.4(a). Another way to determine the wave speed comes up as a side product from analysing the wave form as described above. Both methods are in good agreement with the prediction from the continuum model.

6 Wave propagation across interfaces between two Hertz-like granular crystals with different interaction exponents

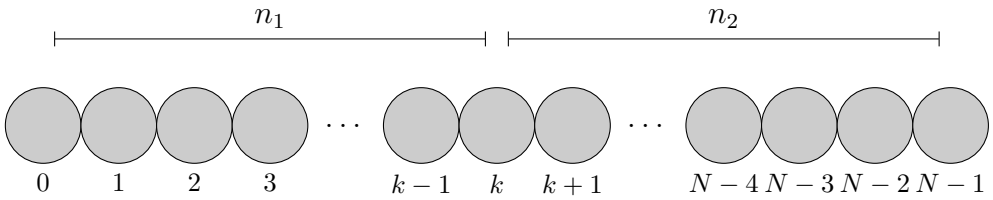

Figure 6.1: Granular chain composed of two media with interaction potential exponents n_1 and n_2 with the interface being at node k. The exponent difference is defined as $\Delta n = n_2 - n_1$. Note that in the experimental implementation the beads are not spherical in general.

As mentioned in Chapter 3, the propagation of solitary waves in granular chains across interfaces between media with different bead masses has been studied extensively [7]. Effects including reflection, transmission and emerging multipulse structures have been found and used to design composite materials for manipulating the propagation behaviour of incoming solitary waves [15, 16, 36, 39, 53].

In this chapter we present a new way of creating interfaces between two types of granular crystals that offers an alternative method of affecting solitary wave propagation in composite media. Knowing that differences in bead masses can induce complex dynamics at interfaces, we want to investigate how abrupt changes in the interaction potential influence the wave propagation. While there are some results for interfaces between linear and non-linear media [7], we are not aware of any work on interfaces between media with different nonlinearities. Therefore, in this chapter we study the propagation properties for solitary waves travelling across interfaces

between media with different interaction exponents n.

The underlying physical property causing the interface effects for mass interfaces is the inertia of the beads, *i.e.* the resistance to acceleration, for which the bead mass is a measure. These differences in acceleration behaviour lead to a disruption of the compression wave propagation causing the opening and closing of gaps and compression imbalances in the vicinity of the interface.

The parameter n governs the shape of the interaction potential and thereby the shape of the interparticle force, as depicted in Figure 2.3. And since according to Newton's second law of motion the force is proportional to the acceleration of the particles we expect imbalances in the acceleration behaviour of the beads at the interface. Therefore, disruptions of the solitary wave propagation are expected in this case as well.

Similarly to mass interfaces, the interface effects for different interaction exponents depend on whether the exponent increases or decreases along the propagation direction. We characterise interfaces by the difference $\Delta n = n_2 - n_1$ between the exponents in the two media.

6.1 Increasing interaction exponent along propagation direction

Figure 6.2(a) shows the bead velocities before and after the solitary wave hits an interface with $n_1 = 3.0$ and $n_2 = 3.5$. For interfaces with $\Delta n > 0$ we observe that most of the energy is transmitted to the medium on the right-hand side; however, there is one additional transmitted pulse and one reflected pulse, both about an order of magnitude smaller in peak velocity[G]. A noteworthy behaviour is that the bead velocities in the vicinity of the interface freeze in a few configurations before all the energy is propagated away from the interface.

Whereas the arriving wave in the medium on the left immediately induces a wave of similar amplitude in the medium on the right, the two secondary pulses are delayed, *i.e.* they do not propagate away from the interface directly after the initial solitary wave hits it, but they freeze close to the interface for some time. This is due to the time it takes to close gaps between beads close to the interface that emerge upon the solitary wave hitting the interface, as shown in Figure 6.2(b).

After the initial wave hits the interface at time t_1, indicated in Figure 6.2(b), the emerging gaps lead to bead 49 freely travelling forward while bead 50 is travelling

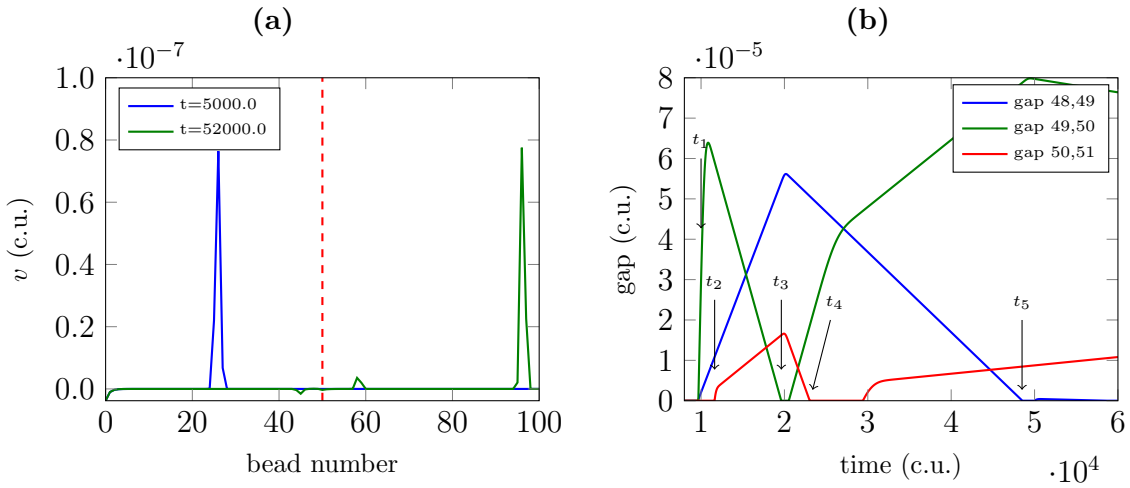

Figure 6.2: Solitary wave propagation across an interface between media with $n_1 = 3.0$ and $n_2 = 3.5$: waves before and after hitting the interface (a) and gaps emerging in the vicinity of the interface (b). In (a) the interface is indicated by the dashed red line.

backwards (*cf.* Figures 6.3(a), 6.3(b)). The beads at the interface are frozen in this state between times t_2 and t_3, when beads 49 and 50 exchange momenta in an elastic two-body collision (*cf.* Figure 6.3(c)). This new state is again frozen until time t_4, when bead 50 closes the gap to its right neighbour and induces the secondary transmitted wave (*cf.* Figure 6.3(d)). The reflected wave starts propagating away from the interface at time t_5 when bead 49 reaches its left neighbour, as shown in Figure 6.3(e). Similar delays have previously been reported for granular containers with mass interfaces [16].

Bead 50 travelling backwards and thereby inducing the small reflected wave is essentially an instance of chain fragmentation in the the right-hand side medium. When the initial solitary wave hits the interface at time t_1 a gap between bead 49 and bead 50 opens, and therefore the two media are disconnected. Hence, similarly to the case discussed in Chapter 5, bead 50 acts as a striker that hits the right medium inducing a solitary wave and chain fragmentation with some beads rebounding in the other direction.

Since the opening and closing of gaps is essential for the explanation of the secondary waves that emerge for interfaces with $\Delta n > 0$, we do not expect them to be captured by any continuum model, as gaps are a feature of the discreteness of granular crystals.

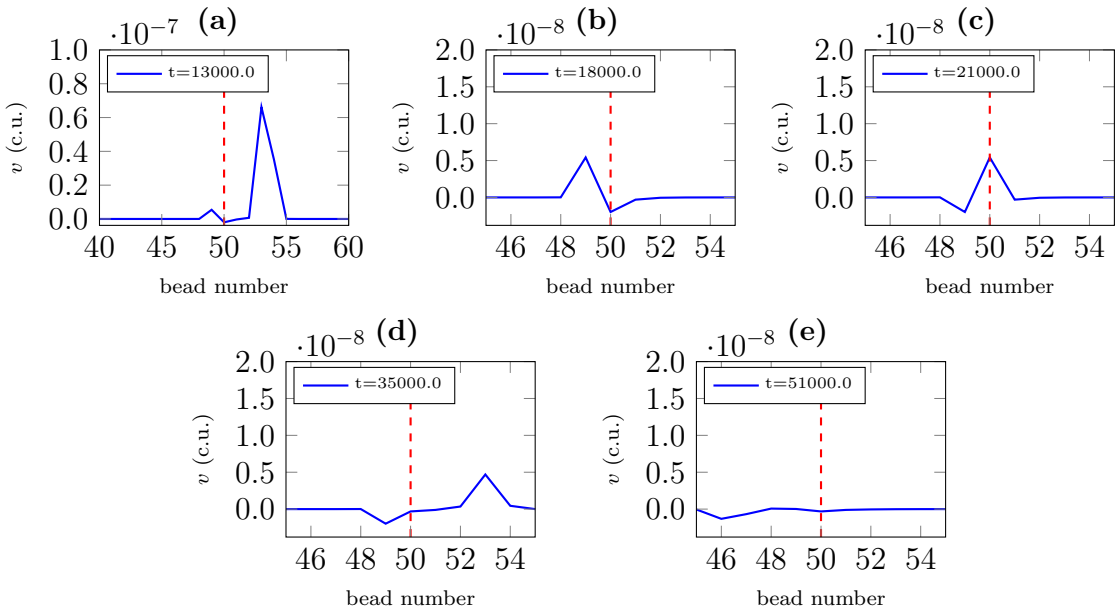

Figure 6.3: Solitary wave propagation across an interface between media with $n_1 = 3.0$ and $n_2 = 3.5$. The interface is indicated by the dashed red line.

6.2 Decreasing interaction exponent along propagation direction

For a wave propagating across an interface with $\Delta n < 0$ the effects are quite different[H]. Figure 6.4(a) shows the bead velocities before and after the initial solitary wave hits the interface for $n_1 = 3.0$ and $n_2 = 2.5$. There is a significant reflection and transmission, with the transmitted energy being converted into a multipulse structure. Unlike in the case discussed above, there is no delay of transmitted or reflected part of the wave.

At the moment when the reflected wave starts to propagate away from the interface, the transmitted energy forms a pulse with a nearly rectangular shape. In the case shown here this means the first 8–9 beads behind the interface have roughly the same velocity (*cf.* Figure 6.4(d)). This nearly rectangular pulse splits and goes on to form the transmitted multipulse structure (*cf.* Figures 6.4(e)–(f)).

In previous numerical simulations it was observed that for rectangular initial conditions, *i.e.* the first l particles having the same initial speed, a multipulse structure with l waves emerges [6, 52]. The transmitted pulse in Figure 6.4(d) resembles such initial conditions for the medium right of the interface.

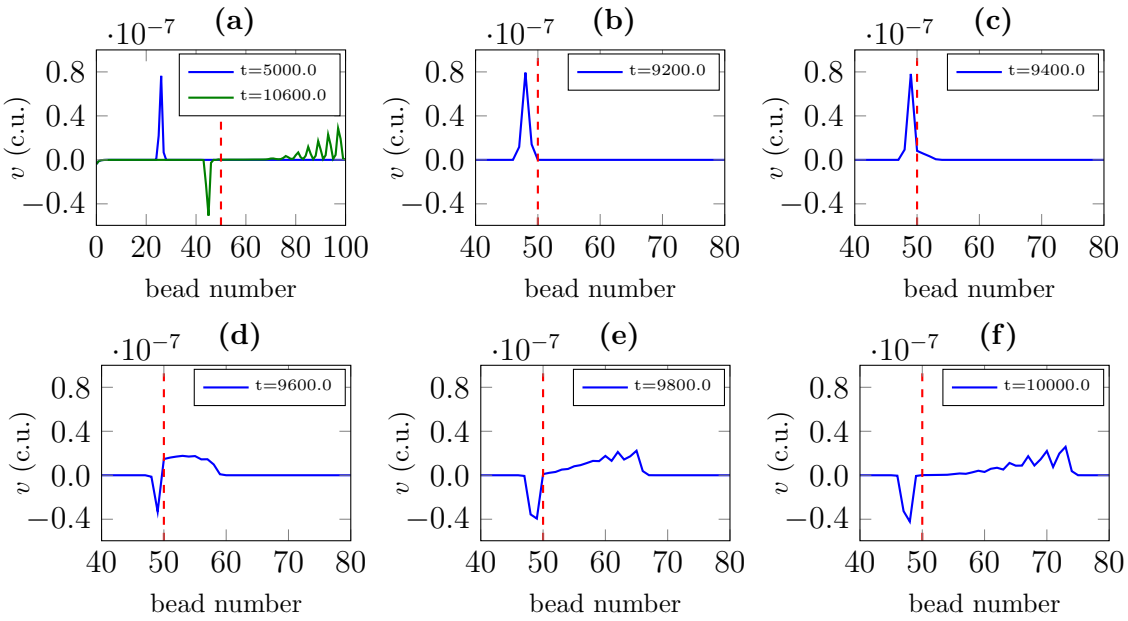

Figure 6.4: Solitary wave propagation across an interface between media with $n_1 = 3.0$ and $n_2 = 2.5$.

The reflected energy propagates away from the interface in the form of a single solitary wave, whose energy can be measured easily. We determine the range of beads that form the solitary wave by finding the beads with more than 0.1% of the peak bead velocity in the wave. As the energy carried by the wave is not purely kinetic, we also need to consider the potential energy stored in the interaction between the beads. Then for a solitary wave which is made up of s beads starting at the k^{th} bead, the wave energy is given by

$$E = \sum_{i=k}^{k+s} m_i v_i^2 + \sum_{j=k}^{k+s-1} a\delta_{j,j+1}^{n_1}, \tag{6.1}$$

where the first and second sum are the kinetic and potential energy carried by the wave respectively. The fraction of reflected energy $E_{\text{refl}}/E_{\text{in}}$, where E_{refl} and E_{in} are the reflected and initial energy, is shown in Figure 6.5 as a function of n_1 and n_2.

For $\Delta n < 0$, *i.e.* when significant reflection occurs, the contours in Figure 6.5 are linear and collapse around the point $(n_1, n_2) \approx (1.65, 1.65)$, which is outside the plotted domain. Therefore, the reflected energy can approximately be described in terms of a new variable

$$\zeta = \frac{n_1 - 1.65}{n_2 - 1.65}, \tag{6.2}$$

as shown in Figure 6.6.

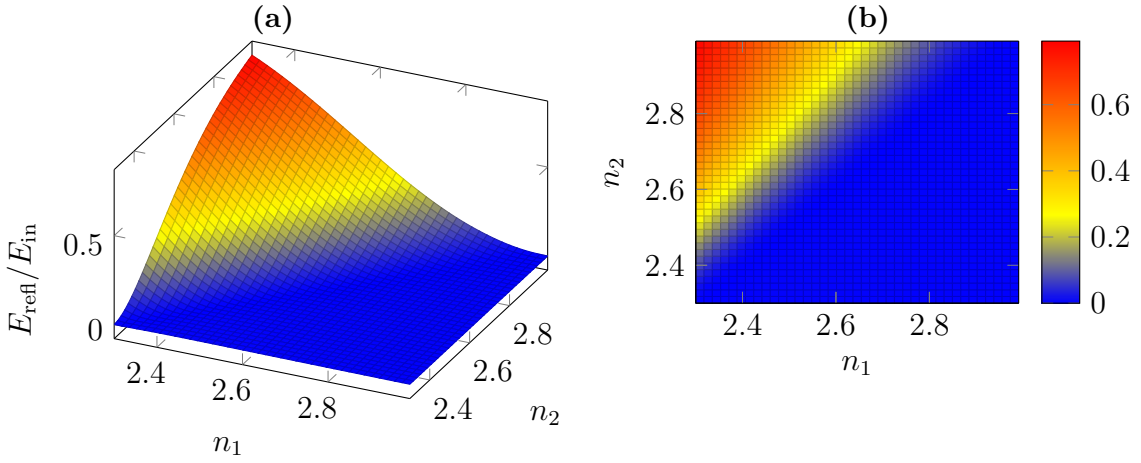

Figure 6.5: Reflected energy as function of n_1 and n_2

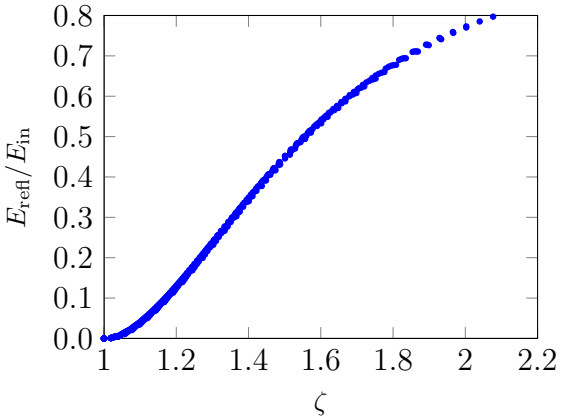

Figure 6.6: Simulated reflected energy as a function of the new variable ζ.

6.3 Two-particle vs. few-particle interactions

Let us consider an interface between media with different bead masses as discussed in [7, 15, 16, 39], more specifically the case where a solitary wave is propagating from the lighter to the heavier medium. As shown in Chapter 5, for large values of n most of the kinetic energy of a propagating solitary wave is carried by a single bead. In this case we can approximate the dynamics to be completely described by at most

two particles interacting with each other at a given point in time, as the velocities of all other particles are essentially zero.

Under these assumptions, the effects arising from the propagation across the interface can be derived from the interaction between the last particle with the lighter mass m at site k, and the first particle with the heavier mass M at site $k+1$ [39]. For such a simple two-body collision the velocities after the collision v'_k and v'_{k+1} are completely determined by the conservation of momentum and energy without having to consider the details of the interaction potential[1]:

$$v'_k = \frac{m-M}{m+M} v_k, \qquad v'_{k+1} = \frac{2m}{m+M} v_k, \tag{6.3}$$

where v_k is the velocity of bead k before the collision and bead $k+1$ is assumed to be initially at rest. As we have $m < M$, bead k moves in the opposite direction causing the reflected wave, whereas bead $k+1$ moves to the right initialising the transmitted wave. A similar two-body argument can be given for the effects arising for a solitary wave propagating in the opposite direction [39].

Returning back to our case of interfaces between regions with different interaction potential exponents n, we can consider the interactions under the same two-body approximation. However, as mentioned above, the details of the interaction are irrelevant for the outcome of a two body collision and since the bead masses are equal we get

$$v'_k = 0 = v_{k+1}, \qquad v'_{k+1} = v_k, \tag{6.4}$$

i.e. the two particles simply exchange momenta. Therefore, in contrast to the mass interfaces, here the reduction to a two-body problem cannot explain any of the observed interface effects. Therefore, all of the observed phenomena must be fundamentally connected to few-body interactions.

This can also be elucidated by recalling that the interface here is constituted by a bead with different interaction potentials on its left and right side, rather than the boundary between two beads, as is true for mass interfaces. Therefore, we need at least three beads to interact in order for the different interaction potentials to play a role in the wave propagation.

At interfaces with $\Delta n < 0$, the number of particles interacting at the interfaces is significantly larger than three. We can define the number of particles that interact at the interface as the number of excited particles just before the reflected and

[1] However we need to assume the inter-particle force is repulsive and conservative, *i.e.* the collision is elastic and no energy is lost.

transmitted waves part. We observe that at the interface the first couple of beads in the right medium are collectively excited by the collision with the incoming solitary wave, as shown in Figure 6.4. In the collision process these collectively excited beads in the right-hand side medium can be imagined as forming a quasi-particle with a mass equal to the sum of its constituent bead masses. The incoming wave accelerates several particles in the right medium simultaneously and is then reflected off this quasi-particle, due to its heavier mass.

The number of particles involved in the interaction at the interface might also be the explanation for the decrease in reflected energy when n is increased uniformly on both sides. For larger n, the wavelength and therefore the number of particles involved in the formation of quasi-particles are smaller, which thereby could decrease the reflection.

6.4 Chains with impurities

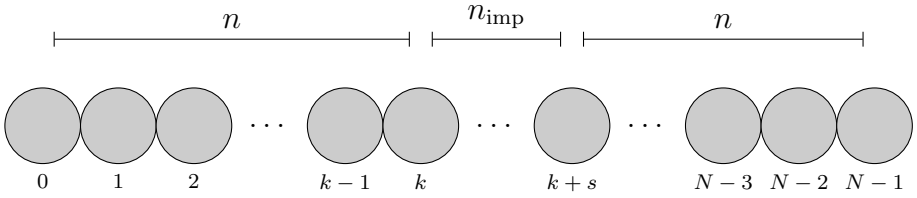

Figure 6.7: Granular chain with interaction exponent n with an impurity of s neighbour interactions with exponent n_{imp}.

Knowing that the abrupt changes in the interaction exponent between two media can cause complex wave propagation phenomena, one might ask what happens when there is a change in the interaction exponent in a localised region within an otherwise monodisperse chain. We consider the situation depicted in Figure 6.7, in which the force between s consecutive bead-bead pairs within the chain is governed by the interaction exponent n_{imp} which are embedded in a chain with interaction exponent n. In this set-up, $s+1$ beads have at least one interaction with a neighbouring bead with the exponent n_{imp}. In order to distinguish impurities from interfaces, we denote the difference in the exponent between the medium and the impurity as $\delta n = n_{\text{imp}} - n$.

Figure 6.8 shows two examples of granular crystals with impurities for $\delta n > 0$ and $\delta n < 0$. Upon hitting the impurity, the initial solitary wave is partially reflected with the remaining energy being converted into a multipulse structure[IJ]. In contrast to

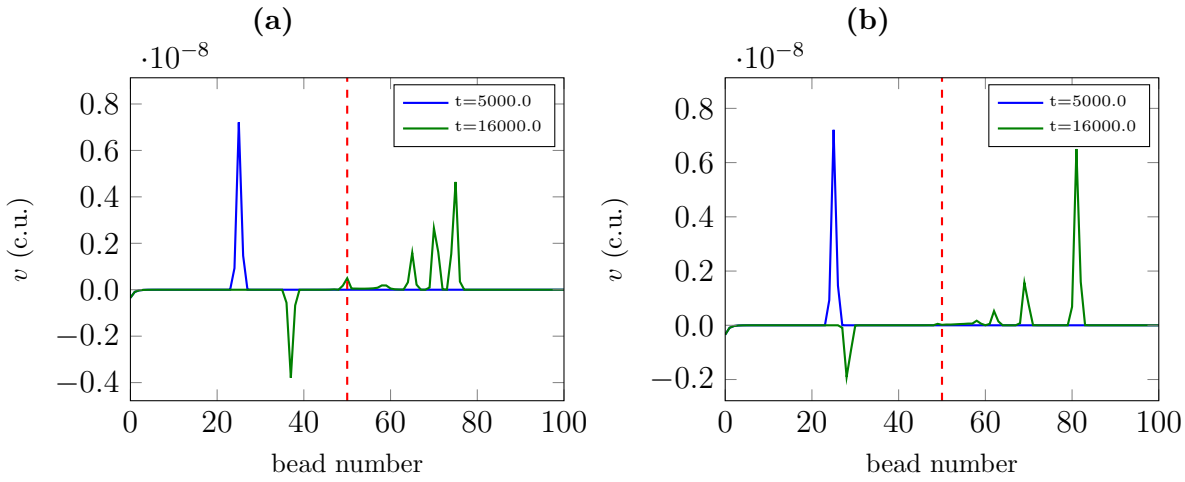

Figure 6.8: Granular crystals with impurities with $s = 1$, $n = 3.0$ for $n_{\text{imp}} = 3.5$ (a) and $n_{\text{imp}} = 2.5$ (b). The red dashed line indicates bead k (*cf.* Figure 6.7).

interfaces, here we obtain similar qualitative behaviour independently of the sign of δn.

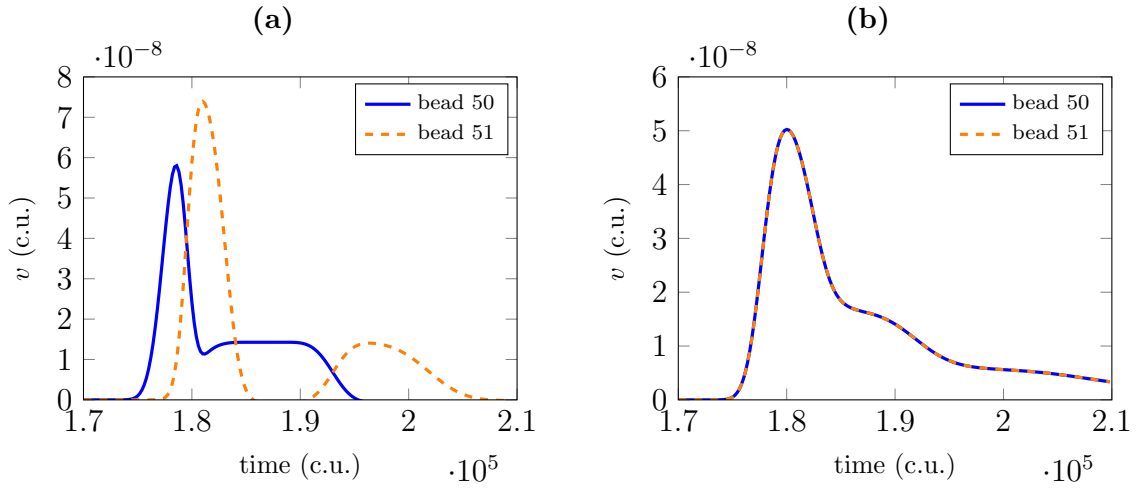

Figure 6.9: Impurity bead velocities with $n = 4.0$ and $s = 1$ for $\delta n = -0.25$ (a) and $\delta n = -1.5$ (b). The two lines are not distinguishable in (b).

An interesting observation we make is that for large negative δn, the impurity beads behave collectively, *i.e.* their velocities are identical. Figure 6.9 shows two examples for the impurity bead velocities during the interaction with the incoming solitary wave for $s = 1$. Whereas for $\delta n = -0.25$ there is an asymmetry between the two impurity beads, they are completely synchronised for $\delta n = -1.5$. This clearly shows

quasi-particle behaviour in which the two impurity beads act as one particle of mass $2m$, similar to the observations for interfaces.

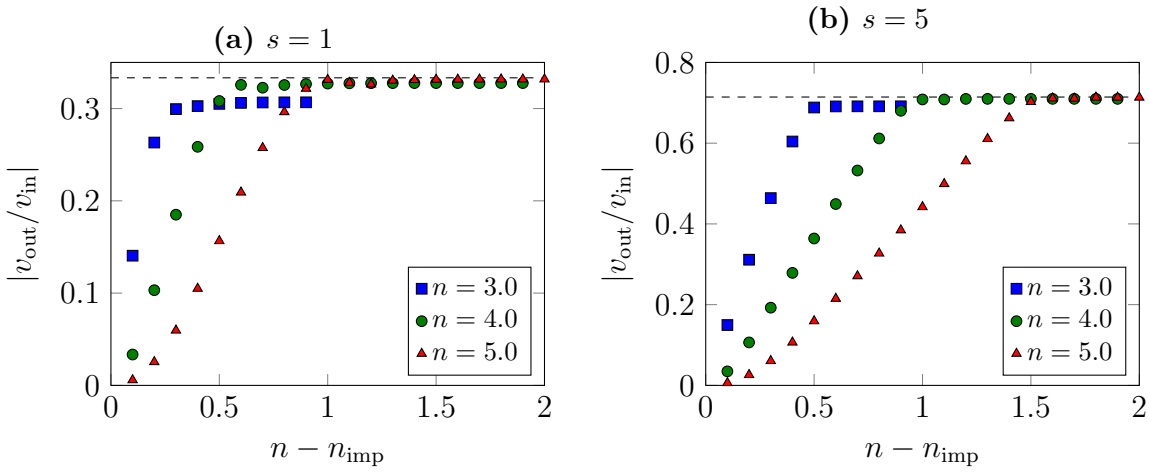

Figure 6.10: Ratio of the peak bead velocities between reflected and incoming solitary wave for impurities with different numbers of impurities s. The dashed line indicates the velocity of a bead with mass m scattering of a bead with mass $(s+1)m$.

We can compare the collision of the solitary wave with the impurity to the two-body approximation as discussed in Section 6.3. Figure 6.10 shows the the ratio of the peak bead velocities between reflected and incoming solitary wave $|v_{\text{out}}/v_{\text{in}}|$ for different values of n and s. For large interaction exponent differences between the medium and the impurity, the reflected velocity converges to the velocity one would get from a particle with mass m colliding with a particle of mass $(s+1)m$ at rest. Therefore the process of the solitary wave interacting with an impurity is described well by the quasi-particle model. For small values of n the reflected velocity does not quite reach the value predicted by the two-body approximation. This is due to the fact that the incoming wave has a larger wavelength, hence approximating it by the motion of a single bead is inaccurate.

6.5 Stability under system perturbations

The analysis of the dynamics of the beads in the vicinity of the interface shows that the numerically observed phenomena depend on the timing of gaps opening and closing and on the shape of the initially transmitted pulse. In experimental set-ups, the conditions might not be as well-controlled as in the numerical simulation due to

the finite precision of the experimental apparatus. In order to investigate the stability of the previously observed effects under small perturbations of the chain parameters, the interaction potential exponent is randomly perturbed by

$$n_i^{\text{pert}} = n_i + n_i^{\text{rand}}, \qquad i \in \{0, \ldots, N-2\}, \tag{6.5}$$

where n_i is the initial exponent and n_i^{rand} is taken from a Gaussian distribution with standard deviation σ and mean 0. However, the additional constraint $n_i^{\text{pert}} > 2.0$ is imposed in order to stay in the non-linear regime. The interaction exponent difference $\Delta n = n_2 - n_1$ provides a scale to which the introduced randomness can be compared.

Figure 6.11 shows the effect of the perturbation for the propagation of a solitary wave across an interface with $\Delta n > 0$. The first observation is that by introducing the perturbation, smaller waves behind the solitary wave develop, even in the monodisperse part of the chain. These smaller waves interfere with the two delayed secondary waves propagating away from the interface. However, a similar qualitative behaviour of the delayed secondary waves is observed up to the point where the smaller waves arising from the perturbations are of comparable size. Secondly, the gaps arising near the interface, which are responsible for the delayed transmitted and reflected secondary pulses, close faster due to interactions with waves arising from the impurities.

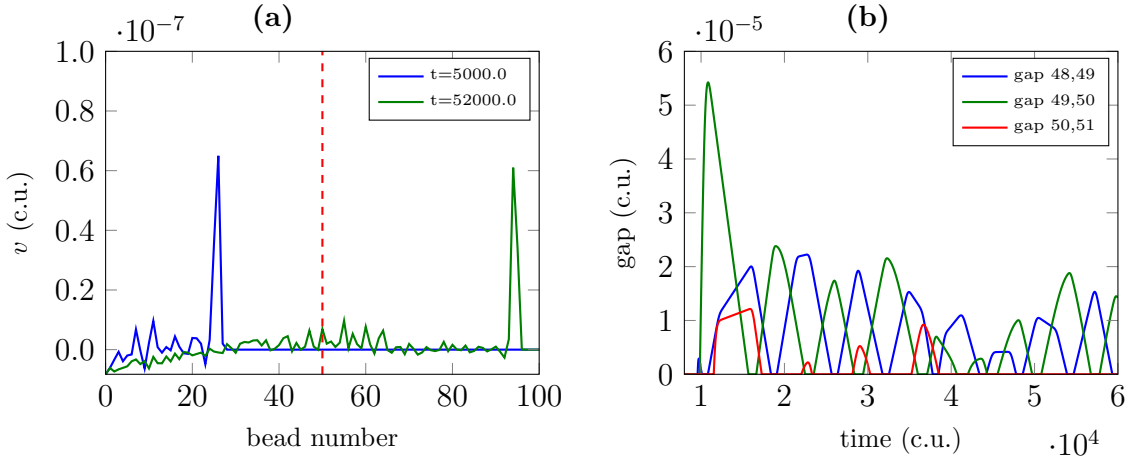

Figure 6.11: Effect of perturbation (6.5) for an interface with $\Delta n > 0$, given $\sigma/\Delta n = 0.05$ ((a), (b)).

The effects of perturbation (6.5) on the propagation across an interface with $\Delta n < 0$ are shown in Figure 6.12. We observe that the initial rectangular pulse, which causes

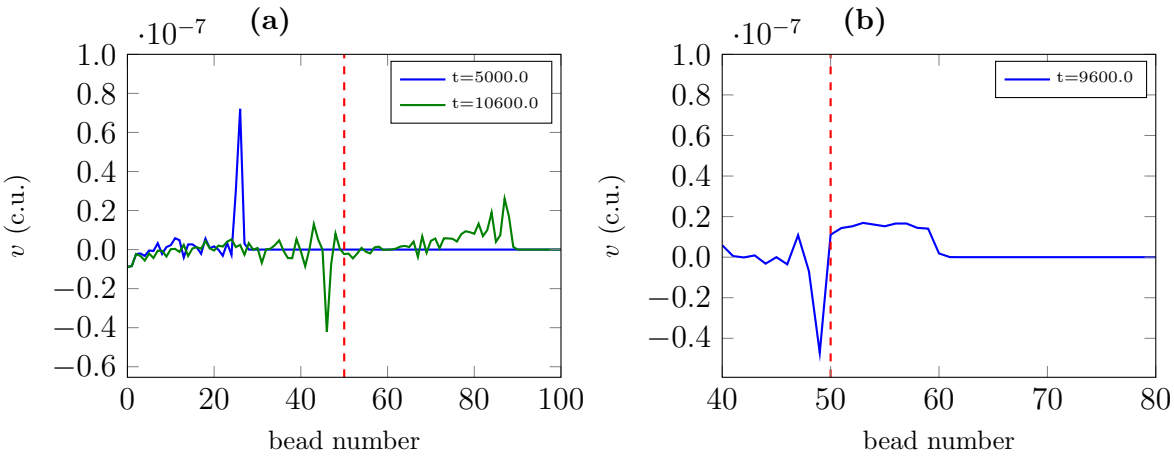

Figure 6.12: Effect of perturbation (6.5) with $\sigma/\Delta n = 0.05$ on solitary wave propagation across an interface between media with $n_1 = 3.5$ and $n_2 = 3.0$: waves before and after hitting the interface (a) and collective excitation of the beads in the right medium (b). The interface is indicated by the dashed red line.

the transmitted multipulse structure, develops for all tested perturbation strengths. Again, the agreement with the unperturbed case is determined by the relative sizes of smaller waves induced by the perturbations and the features arising from the interface, such that the leading peaks of the multipulse structure are clearly visible even for relatively large perturbations whereas the smaller tail is lost in the noise.

For $\Delta n > 0$ the observed interface phenomena are present for perturbations of up to 1% of the interaction potential difference Δn, whereas the multipulse structure and wave reflection for $\Delta n < 0$ are present for perturbations of more than 5%. Therefore, we expect the effects at interfaces between different interaction potentials to be obtainable experimentally for both $\Delta n > 0$ and $\Delta n < 0$.

6.6 Combination of mass and interaction exponent interfaces

Now that we know about the effects of both mass and interaction exponent interfaces, we can study how the combination of both types of interfaces influences the solitary wave propagation. In order to keep the parameter space manageable, we fix the parameters of the left medium to $n_1 = 3.0$ and bead mass $m_1 = m$ as used in the previous simulations, and only change the parameters for the right medium. We vary Δn in $[-0.5, 0.5]$ and the ratio m_2/m_1 between the bead mass on the left and on the

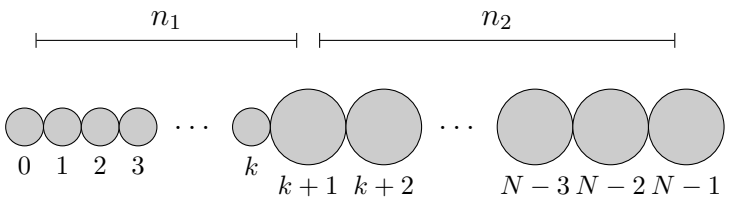

Figure 6.13: Combined mass and interaction exponent interface. Note that the mass on the right-hand side can also be smaller than on the left.

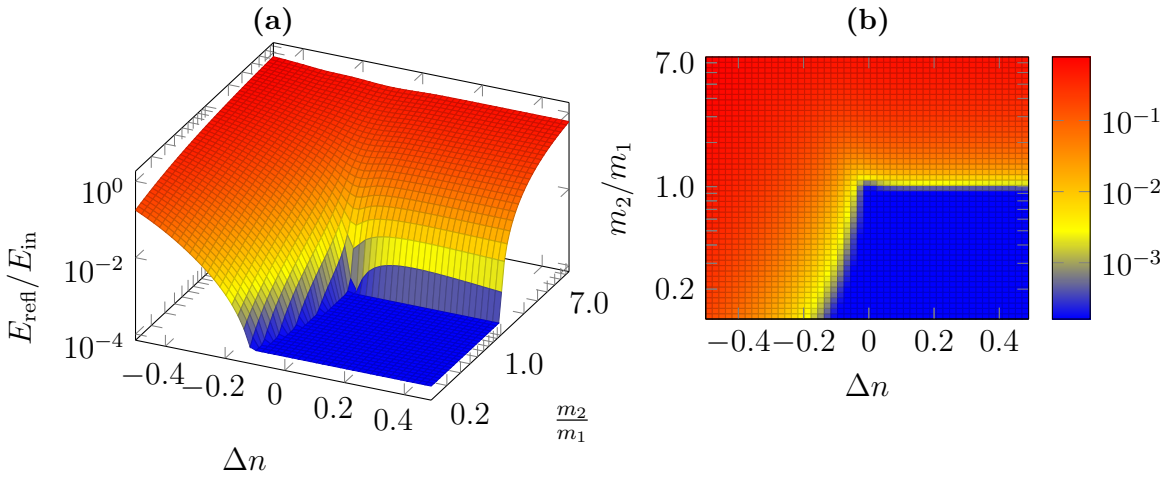

Figure 6.14: Reflected energy as function of Δn and m_1/m_2.

right in $[1/8, 8]$.

Figure 6.14 shows the reflected energy as a function of the two interface parameters. Note that for visualisation purposes where no reflection was detected the value for the reflected energy was set to the minimum value detected over the entire parameter range. Therefore, for the entire dark blue area in the plot, no significant reflection could be detected.

In the bottom-right part of Figure 6.14(b) there is no reflection; this is what we would expect from what we know of both types of interfaces in this parameter regime. Similarly, for the parameters in the top left corner both types of interfaces separately show reflection, which is also the case for the combined interface. In the top-right corner, *i.e.* for $\Delta n > 0$ and $m_2/m_1 > 1$, the reflection is mainly determined by the mass difference with significant reflection for all $m_2/m_1 > 1$. This seems plausible as the difference in interaction exponents for $\Delta n > 0$ had only small effects on the wave propagation.

However, for $\Delta n < 0$ and $m_2/m_1 < 1$, we arrive at contradicting predictions using

our knowledge from the separate study of these two types of interfaces: for mass interfaces we expect a full disintegration of the wave without any reflection, but for interaction exponent interfaces we would predict the emergence of a multipulse structure with significant reflection. For the combined interface we observe a transition between regions with and without reflection. The contour at which the transition occurs can be interpreted in the framework of the quasi-particle model: it is the set of parameters where the effective mass of the quasi-particle on the right-hand side and the bead mass on the left-hand side are equal. In other words, the mass difference in the quasi-particle collision is balanced out by the difference of the bead masses m_1 and m_2.

7 Disorder and periodicity in the interaction exponents

After studying the wave propagation across single interfaces between granular crystals with different interaction exponents, we now want to look at the effects on the wave propagation dynamics of changing the interaction exponents on all pairs of beads independently. We introduce these variations in the interaction exponent in two different ways: by randomly selecting exponents and by periodically alternating between two values. Such set-ups can be seen as the limit of many interfaces, where the media between the interfaces are made up of only single beads.

7.1 Disorder

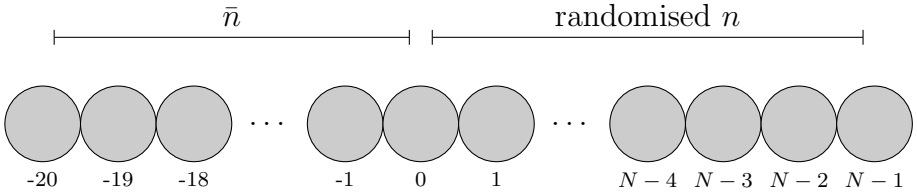

Figure 7.1: Set up of the granular chain for the simulation of solitary wave propagation under randomised n. The first 20 beads constitute a monodisperse chain and the randomisation starts from bead 0. In the simulations $N = 1000$ was used.

As discussed in Chapter 3, solitary waves propagating through a granular chain with randomised masses experience exponential decay. In [39] the masses are set to

$$m_i = \bar{m}\,(1 + r_i\sigma)\,, \qquad i \in \{0, \ldots, N-1\}, \tag{7.1}$$

with $\bar{m}$ being the mean mass, r_i being a random number that is uniformly distributed in $[-1, 1]$, and σ a parameter weighting the randomness of the masses. It could be

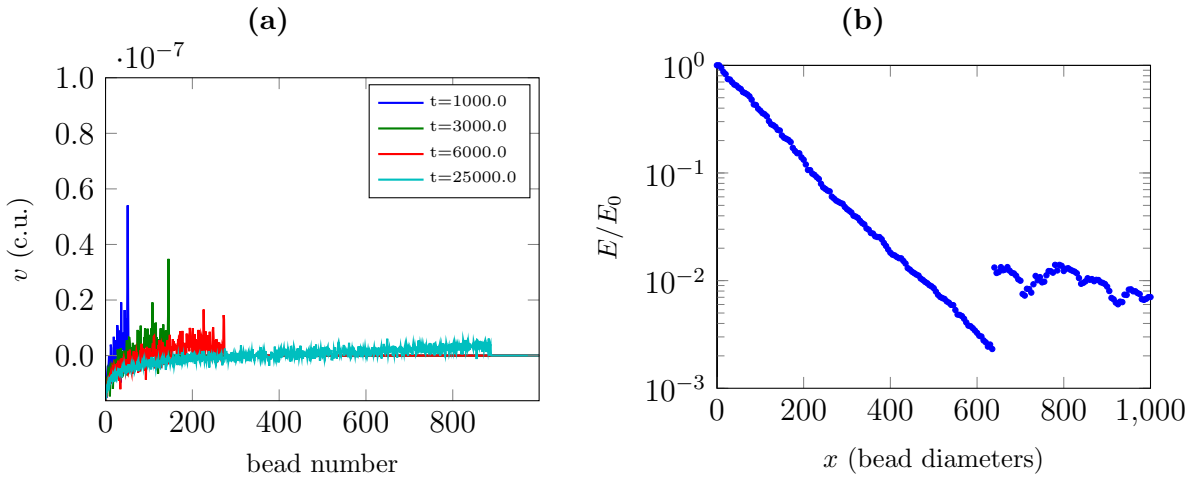

Figure 7.2: Decay of the solitary wave energy in a chain with disorder in the interaction exponents for $\bar{n} = 2.5$ $\epsilon = 0.04$.

observed that the solitary wave energy E decays as

$$E(x) = E_0 \exp(-\alpha_E x), \tag{7.2}$$

where E_0 is the initial energy, x is the position in the chain and α_E is the decay rate. Furthermore, it was found that $\alpha_E \propto \sigma^2$ for small enough σ.

In this Chapter we investigate chains with randomised interaction potential exponents where

$$n_i = \bar{n} + r_i \epsilon, \qquad i \in \{0, \ldots, N-1\}, \tag{7.3}$$

with the mean exponent $\bar{n}$, $\epsilon > 0$ and r_i defined as for (7.1). Whereas the scenario studied in [39] corresponds to a chain of beads with randomised sizes, the case we consider here corresponds to a chain with randomly varying contact surface geometries between the beads.

In order to avoid chain fragmentation effects in the simulation, the chain is set up as shown in Figure 7.1 with a monodisperse chain of 20 beads at the beginning of the chain. In this set-up, the solitary wave can develop before it reaches the part of the chain with randomised n, so that its energy can be measured before the decay.

7.1.1 Numerical Results

The propagation of the solitary wave through a medium with randomised interaction potentials is shown in Figure 7.2(a). As for chains with disordered masses [39], the

initial solitary wave leaves a trace of fluctuating bead velocities behind, to which it continuously looses energy as it traverses the chain[K]. We can quantify the decay of the solitary wave by measuring the total kinetic and potential energy it carries, using the method described in Section 6.2. The energy of the solitary wave relative to the initial energy E/E_0 is shown in Figures 7.2(b) and 7.3. Furthermore, as we have uniform bead masses and the energy is conserved in the system, the bead velocities in the fluctuations right behind the leading wave are smaller than than its maximum bead velocity.

Due to the non-linear nature of waves in granular chains, the trailing fluctuations are slower and do not interact with the leading wave once they have separated. However, once the leading wave has lost enough energy it becomes smaller than fluctuations that have earlier been induced by the leading wave. Therefore, these earlier fluctuations can overtake the leading wave. Hence, for long enough propagation distances, the leading wave is indistinguishable from the induced fluctuations, at which point one can say that the initial solitary wave has fully disintegrated. The jump in the energy of the leading pulse in Figure 7.2(b) shows the point at which the initial solitary wave is overtaken by fluctuations.

In the framework of shock attenuating materials, this kind of wave disintegration may be favourable over shock attenuators consisting of composite materials. Unlike attenuators using interfaces in composite materials, the energy that is extracted from the wave is almost uniformly distributed over all degrees of freedom in the chain. This reduces the maximal single impact at the right end of the chain for fully disintegrated waves.

We observe that the induced fluctuations depend on the size of the leading solitary wave, *i.e.* larger waves cause larger fluctuations. This translates to the energy loss depending on the energy of the leading wave. Figure 7.3 shows the energy of the leading wave as a function of distance travelled in the chain. We can conclude that the energy loss per unit distance travelled is proportional to the wave energy as it decays exponentially.

The straight lines in Figure 7.3 are the result of a least-squares fit of an exponential decay function

$$f(x) = a\mathrm{e}^{-\gamma x}, \tag{7.4}$$

to the wave energy, where the wave energy is given relative to the initial wave energy and the travel distance x is given in units of bead diameters. In our units the decay rate γ is the decay of the wave energy per traversed bead. The deviations from

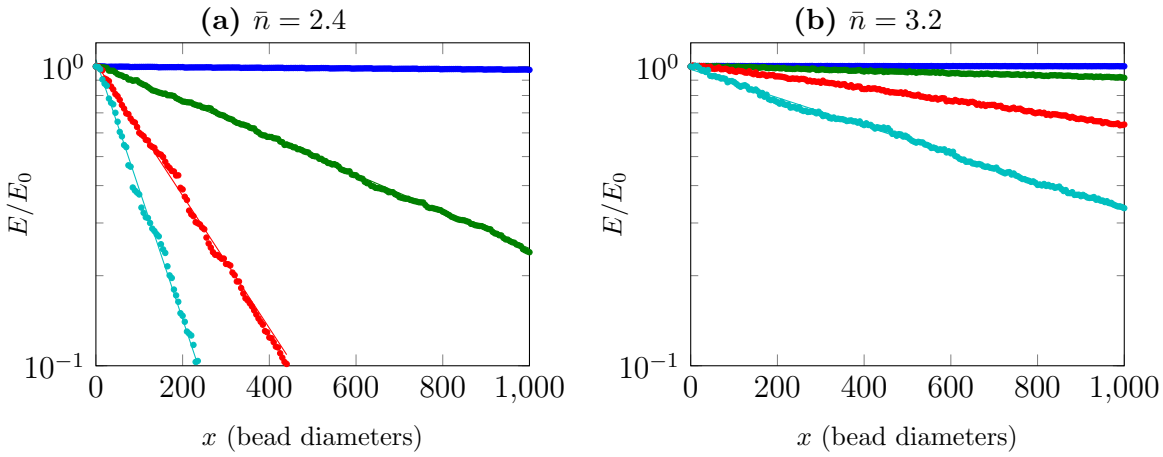

Figure 7.3: Wave decay in chain disorder in the interaction potential exponents for different values of average interaction potential $\bar{n}$ and with randomness parameters ϵ: 0.002 (■), 0.014 (■), 0.026 (■) and 0.04 (■). The travel distance is given in units of the bead diameter. The dots represent the simulation data and the solid lines are fitted exponentials.

Parameter	Value	$\sqrt{\sigma}$
α	2.08453172	0.0079
$\tilde{B}$	−3.51075448	0.014
$\tilde{C}$	10.94456937	0.077

Table 7.1: Fit parameters of the fit function in Equation (7.6).

the exponential decay come from the randomness of the interaction exponent in the chain, which causes inhomogeneities in the n-differences between beads along the propagation direction.

The decay rate as a function of the randomness ϵ and $\bar{n}$ is shown in Figure 7.4. We observe the following relations

$$\log(\gamma) \propto \log(\epsilon), \qquad \log(\gamma) \propto \bar{n}, \tag{7.5}$$

from which we infer the ansatz for a logarithmic model for $\gamma(\epsilon, n)$ as

$$\log(\gamma) = \alpha \log(\epsilon) + \tilde{B}\bar{n} + \tilde{C}, \tag{7.6}$$

where α, $\tilde{B}$ and $\tilde{C}$ are parameters which are determined by a least-squares fit. For

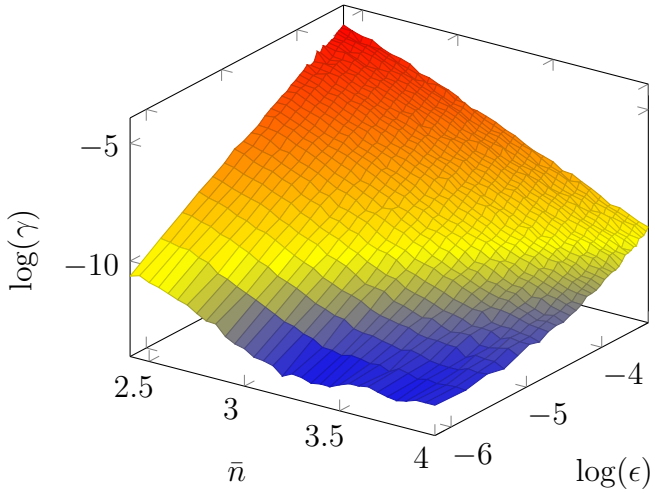

Figure 7.4: Decay rate γ of the solitary wave as function of $\bar{n}$ and ϵ.

the fit we are only using data with $\log(\gamma) > -10$, as for very small decay rates the obtained data is unreliable due to the finite precision of the exponential decay fit through which they are computed. The results for the fit parameters are shown in Table 7.1. We can rearrange Equation (7.6) to obtain

$$\gamma(\epsilon, \bar{n}) = C\epsilon^{\alpha}\beta^{\bar{n}}, \tag{7.7}$$

with $\beta = \exp(\tilde{B}) = 0.030$ and $C = \exp(\tilde{C}) = 56646$. Hence the wave energy decays as

$$E(x) \propto \exp\left(-C\epsilon^{\alpha}\beta^{\bar{n}}x\right). \tag{7.8}$$

Interestingly, we find the same relation between the randomness parameter and the decay rate as in the case for disorder in the bead masses[1], as $\gamma \propto \epsilon^{\alpha}$ with $\alpha \approx 2$.

For the parameters tested here the maximal decay rate is obtained at $\bar{n} = 2.4$, $\epsilon = 0.04$ for which the decay rate (7.7) is $\gamma \approx 0.02$. At this decay rate the wave energy is halved approximately every 15 beads.

Another question one might ask is how the differences in interaction potential influence the energy transmission in the granular chain. As discussed in Chapter 6, the mechanisms that lead to wave reflection at interfaces are few-particle interactions, however, the media in the case of disorder in the chain are reduced to a single particle on each side of the interface. Therefore, the knowledge about the effect of differences in the interaction potential exponent cannot necessarily be transferred to the case of

[1]Note that the different definitions of (7.1) and (7.3) do not affect the exponent of ϵ in the decay rate.

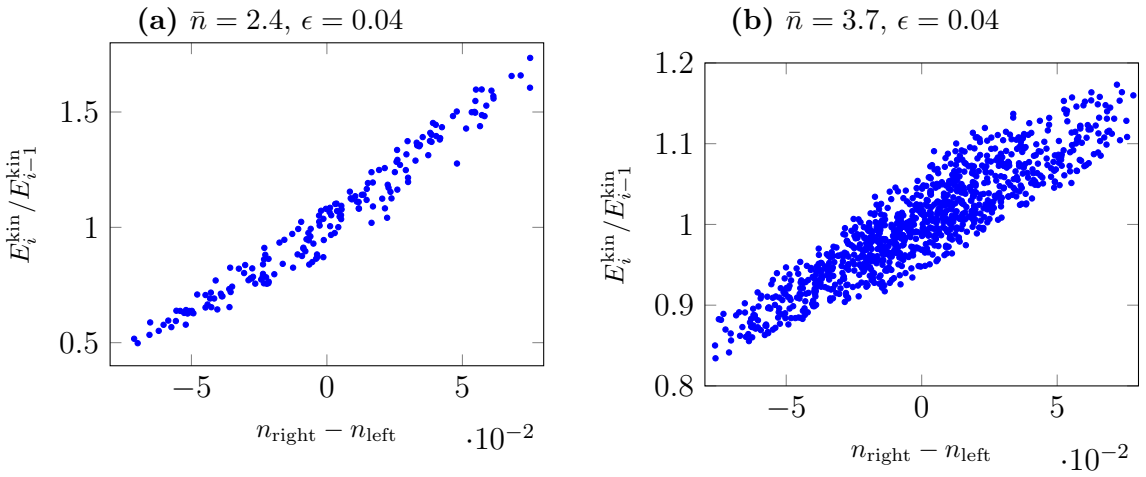

Figure 7.5: Energy transfer from bead $i-1$ to bead i measured by the ratio of maximum kinetic energies $E_i^{\text{kin}}/E_{i-1}^{\text{kin}}$.

disorder.

As a measure of the transmitted energy from bead $i-1$ to bead i, we compare their maximal kinetic energy

$$E_i^{\text{kin}} = \frac{m v_i^2}{2}. \tag{7.9}$$

As shown in Figure 7.5, the difference $n_{\text{right}} - n_{\text{left}}$ between the exponents in the interaction with the right and left neighbour of bead i is a good parameter to describe how much kinetic energy is transmitted to it from bead $i-1$. On average, energy is reflected for $n_{\text{right}} < n_{\text{left}}$, which resembles the case of interfaces between media with different interaction exponents with $\Delta n < 0$. For $n_{\text{right}} > n_{\text{left}}$ bead i reaches an even higher maximum kinetic energy. This can be understood by considering the shapes of the interparticle forces as a function of the bead overlap shown in Figure 2.3. For larger interaction exponents, the force is smaller for small overlaps and increasing more steeply as the overlap is increased. Therefore, early on in the acceleration process, the i^{th} bead is accelerated by bead $i-1$ without transferring much energy to bead $i+1$. In other words, the i^{th} bead has more time to be accelerated before it has to pass on the energy to bead $i+1$. The variance in the energy transfer is in accordance with our findings in Section 6.3 that processes at interfaces between media with different interaction exponents are few-particle processes. Therefore, we expect the energy transfer to not only depend on n_{left} and n_{right}, but also on interactions with other beads close by.

It is remarkable that even though the phenomena at mass and interaction exponent

interfaces are due to different processes, as discussed in Section 6.3, we find the same qualitative behaviour for disorder, which can be seen as the limit of many interfaces. Moreover, we find the same dependence of the decay rate on the randomness parameter. However, in contrast to disorder in the bead masses, we find an additional dependence on the average interaction exponent $\bar{n}$. This additional dependence can be explained by considering the scaling properties of the equation of motion (2.7). Without externally applied forces, changing the overall mass is equivalent to changing the overall time scale of the dynamics, as we can remove any changes in the overall mass by appropriate re-scaling of time. This is not the case for changes of the average interaction exponents.

7.2 Periodicity

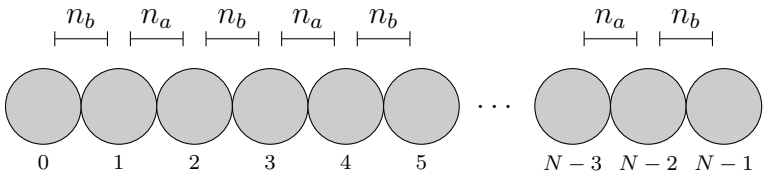

Figure 7.6: Granular chain of spherical beads with alternating interaction potentials.

Another possibility for the implementation of the limit of many interfaces is to periodically alternate between two interaction exponents. As discussed in Chapter 3, granular crystals with alternating bead masses, also callled *dimer* or *di-atomic* granular crystals, show interesting wave propagation properties. Motivated by these results, we want to investigate the effects of periodically changing the interaction exponents in the chain. More specifically, in this section we study the wave propagation in granular crystals in which the interaction exponent is alternating between two values, n_a and n_b, as depicted in Figure 7.6. We denote the difference between the two interaction exponents as $\mathrm{d}n = n_b - n_a$.

7.2.1 Numerical results

We can distinguish three regimes of $\mathrm{d}n$ with different qualitative behaviour. In the trivial case for $\mathrm{d}n \approx 0$ we recover the behaviour for a monodisperse chain, as discussed in Chapter 5. In the limit $|\mathrm{d}n| \to \infty$, with the constraint $n_a, n_b > 2$, we find pairwise collective behaviour of the beads. Figure 7.7(a) shows the emergence of a solitary wave for a granular crystal with $n_a = 2.5$ and $n_b = 3.0$. A solitary wave is forming

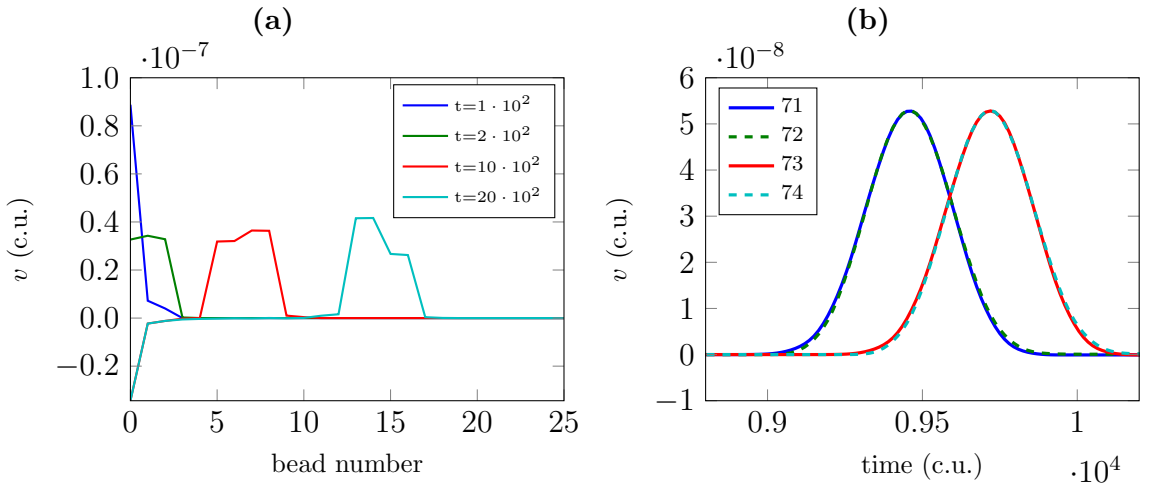

Figure 7.7: Solitary wave with pairwise collective behaviour for $n_a = 2.5$ and $n_b = 3.0$: emergence of solitary wave upon striking the chain from the left (a) and bead velocities for beads 71–74 in the chain (b).

within the first 15 beads, however, neighbouring beads, which interact via a potential with the smaller exponent n_a, move in pairs[L]. Figure 7.7(b) shows the bead velocity for four consecutive beads in the chain. The two bead pairs that interact with the exponent n_a have practically identical velocities. Furthermore, for the qualitative behaviour of the emerging solitary wave it is irrelevant whether the chain starts with n_a or n_b at the left end. The only difference between these cases is the fraction of energy which is lost in the chain fragmentation, where the largest rebound velocity is higher when the chain starts with the smaller interaction exponent.

Generally, for large exponent differences dn, the granular crystal behaves like a chain made up of particles with mass $2m$ interacting via a potential with exponent $\max(n_a, n_b)$. Hence, in this limit, the precise value of the smaller exponent becomes irrelevant.

There is an intermediate regime for $0 < |\mathrm{d}n|$, in which we find similar behaviour to chains with disorder in the interaction exponents[M]. Figure 7.8(a) shows the propagation of a wave for $n_a = 2.5$ and $n_b = 2.555$. The wave energy decays exponentially with the travelled distance, however the leading wave leaves a trail of smaller waves behind which is more regular than for chains with disorder in the interaction exponents. Neighbouring beads which interact via the smaller exponent do not behave collectively, as shown in Figure 7.8(b). However, we do observe that all beads, sufficiently far away from the left end, behave qualitatively similar to beads that have the

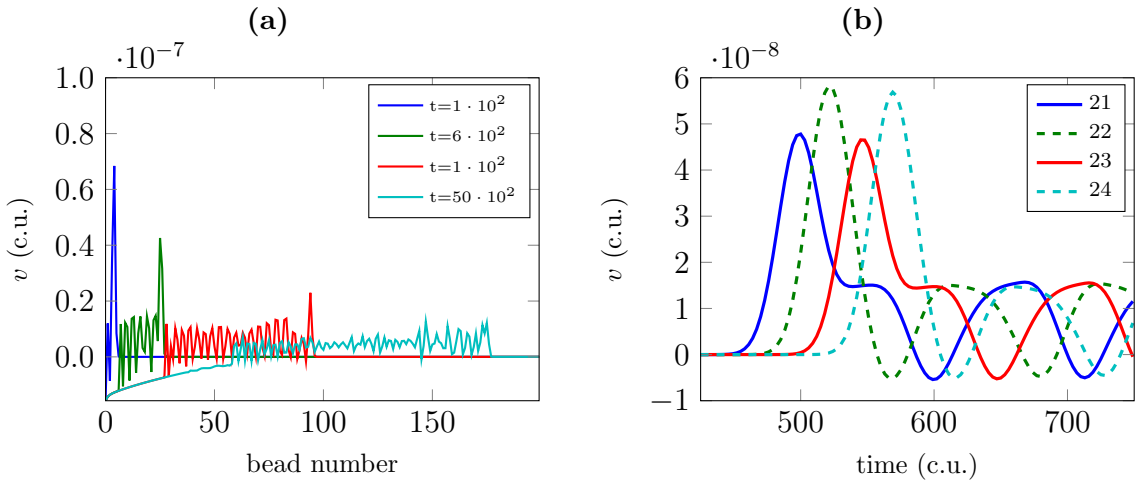

Figure 7.8: Wave decay without pairwise collective behaviour for $n_a = 2.5$ and $n_b = 2.555$: emergence of solitary wave upon striking the chain from the left (a) and bead velocities for beads 21–24 in the chain (b).

same configuration of left and right interaction exponents. In other words, all even beads show qualitatively similar behaviour, and the same is true for all odd beads.

As for the analysis in Section 7.1, we can determine the decay rate through a least-squares fit to the energy of the leading wave. The decay rate is shown for different n_a in Figure 7.9 as a function of $\mathrm{d}n$. As expected the decay rate is zero for $\mathrm{d}n = 0$ and tends to zero for large $|\mathrm{d}n|$. However, there are other local minima in addition to the local minimum at $\mathrm{d}n = 0$.

Figure 7.10(a) shows the wave propagation[N] corresponding to the parameters first minimum for positive $\mathrm{d}n$ in Figure 7.9(a). Within around 25 beads we observe the formation of a stable compression wave and smaller separated secondary waves. The dynamics of the beads forming the wave more complex than for other waves we have discussed thus far. In contrast to waves forming in the limit of large $\mathrm{d}n$, the wave emerging here is not of constant shape. Figure 7.10(b) shows the bead velocities for four consecutive beads in the chain. Beads 71 and 72 interact via a potential with the smaller exponent n_a, *i.e.* they correspond to beads that would behave collectively in the limit of large $|\mathrm{d}n|$. We observe that the velocity of the two beads oscillates around their mean, during which the bead with the highest velocity changes three times. Hence, the peak of the wave periodically oscillates between the front and the back of the wave. These changes of the bead with the peak velocity correspond to several small collision-like interactions between beads that form the wave. These

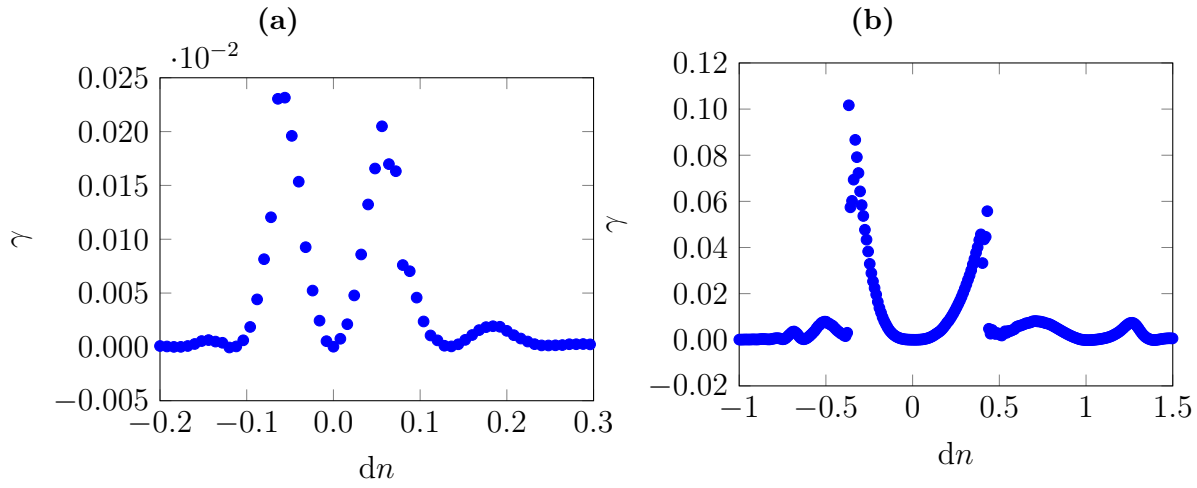

Figure 7.9: Decay rates for periodically arranged interaction exponents with $n_a = 2.5$ (a) and $n_a = 4.0$ (b).

are not full collisions, as the beads in the wave do separate. For the parameters corresponding to the first minimum for negative dn we observe similar behaviour. For $n_a = 4.0$, there is one more minimum in the decay rate at both ends, as shown in Figure 7.9(b). The wave propagation for parameters corresponding to the second minimum are shown in Figure 7.11. The dynamics are similar to the first minimum, however the velocities of the bead pairs oscillate five times around their mean while forming the wave.

The bead velocities shown in Figures 7.10(b) and 7.11(b) show interesting symmetry properties. The velocity profiles of all odd and all even beads are qualitatively and quantitatively the same, only shifted in time. Furthermore, even though the bead pairs interacting via a potential with the smaller exponent do not move collectively, their velocity profiles show a mirror symmetry. This type of wave might not be considered a solitary wave, as the wave shape periodically changing. However, these waves are stable and spatially confined, as for classical solitary waves in granular crystals. We are not aware of any other reports on such stable waves with periodically changing wave shape for granular crystals.

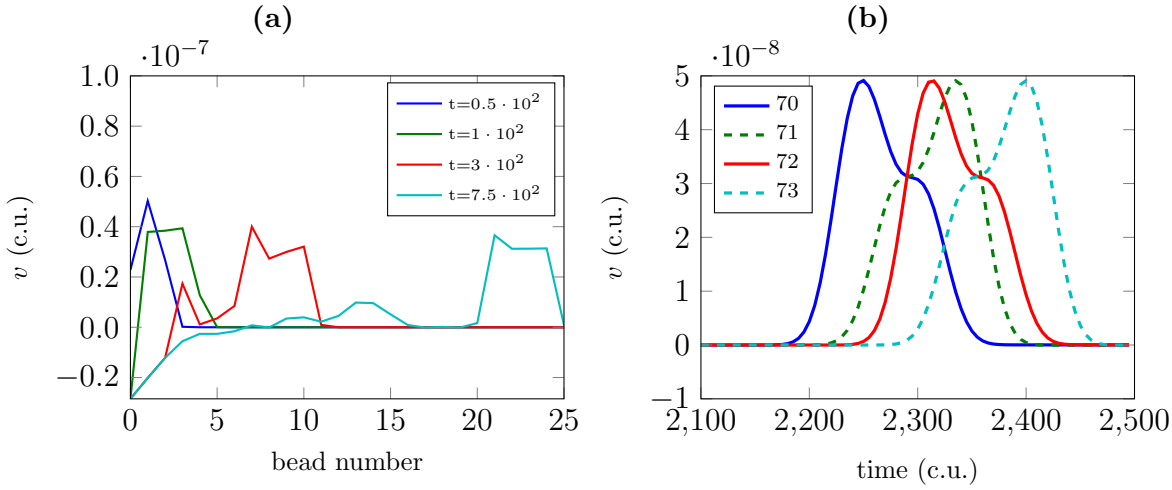

Figure 7.10: Solitary wave with pairwise on resonance for $n_a = 2.5$ and $n_b = 2.635$: emergence of solitary wave upon striking the chain from the left (a) and bead velocities for beads 71–74 in the chain (b).

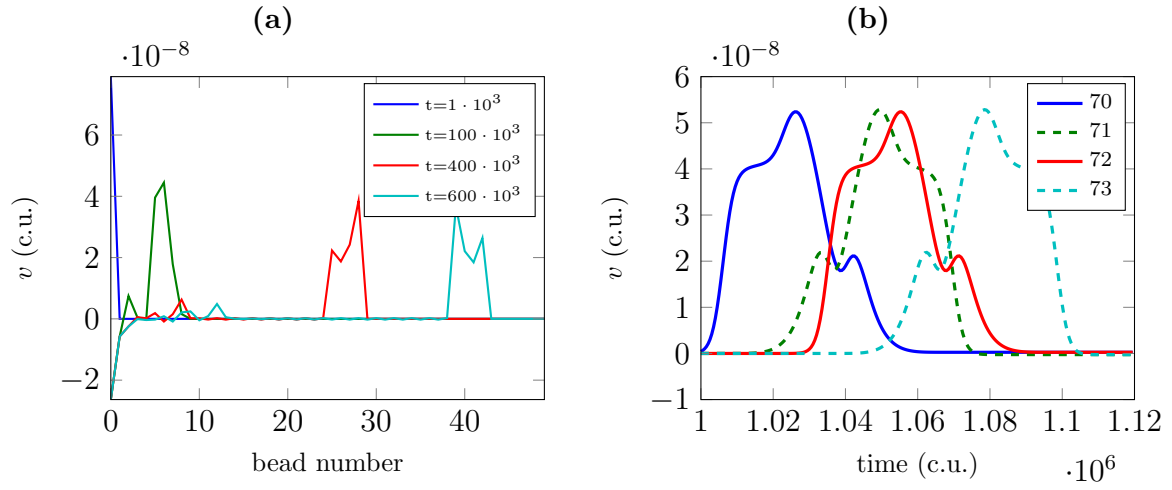

Figure 7.11: Solitary wave with pairwise on resonance for $n_a = 4.0$ and $n_b = 5.0$: emergence of solitary wave upon striking the chain from the left (a) and bead velocities for beads 71–74 in the chain (b).

8 Summary and Outlook

In this dissertation we have presented a numerical study of solitary wave propagation across interfaces in granular crystals with Hertz-like interactions. After reviewing results in the literature for research on interfaces between granular crystals with different bead masses, composite materials, mass disorder and di-atomic granular crystals, we analysed the propagation of solitary waves in monodisperse media under different interaction exponents, comparing an analytical continuum model to numerical simulations.

We have investigated interfaces between media with different interaction exponents n. For $\Delta n > 0$, we obtain mainly transmission of the incoming wave with one transmitted and one reflected secondary wave forming at the interface with a time delay to the primary transmitted wave. The secondary waves are around one order of magnitude smaller in peak bead velocity than the original wave and their formation involves the opening and closing of gaps in the vicinity of the interface. The emergence of these secondary waves is thus a direct consequence of the discreteness of the granular chain. This effect is not expected to be captured by any models using the continuum approximation.

For interfaces with $\Delta n < 0$, both transmission and reflection of the solitary wave occur. Whereas the reflected part of the initial energy propagates away from the interface in form of a single solitary wave, the transmitted energy is converted into a multipulse structure. Combining both mass and interaction exponent interfaces we could find a transition between parameter regimes with and without reflection of the solitary wave. This is in accordance with our explanation for reflection in the absence of bead mass differences for the case of pure interaction exponent interfaces.

Although similarities between the effects at mass and interaction exponent interfaces exist, the underlying dynamics at the vicinity of the interface are fundamentally different. Whereas mass interfaces can be explained in terms of collisions between single beads with different masses, the phenomena at interaction exponent interfaces with $\Delta n < 0$ involve few-body dynamics close to the interface. Moreover, we found that the first few beads on the right-hand side of the interface are collectively accel-

erated causing the partial reflection of the incoming wave. We were able to give a simple interpretation of the process in terms of a quasi-particle collision.

In the investigation of chains with impurities of different interaction exponent we could demonstrate that the collective movement of beads leading to quasi-particle behaviour causes the reflection of incoming solitary waves at the impurity. Moreover, we could show that the peak bead velocity of the reflected wave converges to the prediction in the quasi-particle model for large differences between impurity and chain interaction exponent.

Lastly, we studied the effect of disorder and periodicity in the interaction potentials on the propagation of solitary waves. For randomised interaction potentials, the energy of the waves was found to decay exponentially in space by inducing noise in the bead velocities to which the energy is lost. We were able to find a law for the decay rate in terms of the mean interaction exponent and the randomness parameter. The decay rate scales in the same way with the randomness parameter as for disorder in the bead masses.

In granular crystals with interaction exponents alternating between two values we have identified parameter regimes with qualitatively different wave propagation properties. For large differences between the interaction exponents we find pairwise collective behaviour of the beads, where neighbouring beads interacting via an interaction with the smaller exponent move as pairs forming a solitary wave. For intermediate exponent differences we find mainly exponential decay of the wave energy, similarly to the case of randomised interaction exponents. However, there are certain parameters, for which a different type of stable, confined waves develop, even though the beads do not move in pairs. These waves are different to classical solitary waves in granular crystals, as their wave shape is not constant, but changes periodically.

One question that might be considered for future work is the study of interfaces involving different types of interaction potentials. In this thesis, we have considered interactions that are purely based on contact forces, which lead to Hertz-like power-law potentials. However, one could imagine having additional or different types of interactions between the particles. We are aware of one study using an external magnetic dipole field to introduce additional forces between the beads due to magnetisation. The additional interaction introduces dispersion, which in turn leads to wave attenuation [54]. These different types of interactions could be used to create interfaces which yield interesting wave propagation dynamics.

Another logical step in the study of interfaces between granular crystals with different interaction exponents under contact forces is the generalisation to higher di-

mensions. In higher dimensions the packing of the beads and the direction of the compression wave with respect to the main axes of the granular crystal influence the propagation in monodisperse media [3]. When interfaces are present, higher dimensions offer additional degrees of freedom for the wave propagation, namely the angle at which the wave meets the interface. In 2D a law for the refraction and reflection of solitary waves at mass interfaces similar to Snell's law in optics was found [55]. As we have shown, in 1D there are similarities between the effects arising when solitary waves are propagation across mass and interaction exponent interfaces. Therefore, in 2D there could be similar refraction and transmission effects for interaction exponent interfaces.

Bibliography

[1] User:GeoTrinity. File:kugelstoszpendel.jpg. URL `commons.wikimedia.org`.

[2] H. M. Jaeger, S. R. Nagel, and R. P. Behringer. Granular solids, liquids, and gases. *Rev. Mod. Phys.*, 68:1259–1273, 1996.

[3] M. Manjunath, A. P. Awasthi, and P. H. Geubelle. Plane wave propagation in 2d and 3d monodisperse periodic granular media. *Granular Matter*, 16(1):141–150, 2014.

[4] F. Herrmann and P. Schmälzle. Simple explanation of a well-known collision experiment. *American Journal of Physics*, 49(8):761–764, 1981.

[5] M. A. Porter, C. Daraio, I. Szelengowicz, E. B. Herbold, and P.G. Kevrekidis. Highly nonlinear solitary waves in heterogeneous periodic granular media. *Physica D: Nonlinear Phenomena*, 238(6):666–676, 2009.

[6] V. F. Nesterenko. *Dynamics of heterogeneous materials*. Springer, New York, 2001.

[7] S. Sen, J. Hong, J. Bang, E. Avalos, and R. Doney. Solitary waves in the granular chain. *Physics Reports*, 462(2):21–66, 2008.

[8] Stéphane Job, Francisco Melo, Adam Sokolow, and Surajit Sen. How hertzian solitary waves interact with boundaries in a 1d granular medium. *Phys. Rev. Lett.*, 94:178002, 2005.

[9] W. P. Schonberg, H. A. Burgoyne, J. A. Newman, W. C. Jackson, and C. Daraio. Proceedings of the 2015 hypervelocity impact symposium (hvis 2015) guided impact mitigation in 2d and 3d granular crystals. *Procedia Engineering*, 103: 52–59, 2015.

[10] G. Gantzounis, M. Serra-Garcia, K. Homma, J. M. Mendoza, and C. Daraio. Granular metamaterials for vibration mitigation. *Journal of Applied Physics*, 114(9):093514, 2013.

[11] C. S. Chang and J. Gao. Non-linear dispersion of plane wave in granular media. *International Journal of Non-Linear Mechanics*, 30(2):111–128, 1995.

[12] A. Leonard and C. Daraio. Stress wave anisotropy in centered square highly nonlinear granular systems. *Phys. Rev. Lett.*, 108:214301, 2012.

[13] N. W. Mueggenburg, H. M. Jaeger, and S. R. Nagel. Stress transmission through three-dimensional ordered granular arrays. *Phys. Rev. E*, 66:031304, 2002.

[14] K. L. Johnson. *Contact mechanics*. Cambridge University Press, Cambridge, 1985.

[15] L. Vergara. Scattering of solitary waves from interfaces in granular media. *Phys. Rev. Lett.*, 95:108002, 2005.

[16] L. Vergara. Delayed scattering of solitary waves from interfaces in a granular container. *Phys. Rev. E*, 73:066623, 2006.

[17] D. Khatri, D. Ngo, and C. Daraio. Highly nonlinear solitary waves in chains of cylindrical particles. *Granular Matter*, 14(1):63–69, 2012.

[18] H. Hertz. Ueber die berührung fester elastischer körper. *Journal für die reine und angewandte Mathematik*, 92:156–171, 1882.

[19] L. D. Landau, E. M. Lifšic, J. B. Sykes, and W. H. Reid. *Theory of elasticity*. Pergamon Press, Oxford, 1963.

[20] C. Coste, E. Falcon, and S. Fauve. Solitary waves in a chain of beads under hertz contact. *Phys. Rev. E*, 56:6104–6117, 1997.

[21] G. Friesecke and J. A. D. Wattis. Existence theorem for solitary waves on lattices. *Communications in Mathematical Physics*, 161(2):391–418, 1994.

[22] R. S. MacKay. Solitary waves in a chain of beads under hertz contact. *Physics Letters A*, 251(3):191–192, 1999.

[23] J.-Y. Ji and J. Hong. Existence criterion of solitary waves in a chain of grains. *Physics Letters A*, 260(1–2):60–61, 1999.

[24] J. E. Allen. The early history of solitons (solitary waves). *Physica Scripta*, 57 (3):436, 1998.

[25] P. G. Drazin and R. S. Johnson. *Solitons : an introduction*. Cambridge University Press, Cambridge, 1989.

[26] Clifford S. Gardner, John M. Greene, Martin D. Kruskal, and Robert M. Miura. Method for solving the korteweg-devries equation. *Phys. Rev. Lett.*, 19:1095–1097, 1967.

[27] R. Fedele, B. Eliasson, F. Haas, P. K. Shukla, D. Jovanović, and S. De Nicola. Soliton solutions of the 3D Gross-Pitaevskii equation by a potential control method. 1306:61–74, 2010.

[28] W. Bao, D. Jaksch, and P. A. Markowich. Numerical solution of the gross–pitaevskii equation for bose–einstein condensation. *Journal of Computational Physics*, 187(1):318–342, 2003.

[29] G. Teschl. Almost everything you always wanted to know about the Toda equation. *Jahresber. Deutsch. Math.-Verein.*, 103(4):149–162, 2001.

[30] V. F. Nesterenko. Propagation of nonlinear compression pulses in granular media. *Journal of Applied Mechanics and Technical Physics*, 24(5):733–743, 1983.

[31] A. N. Lazaridi and V. F. Nesterenko. Observation of a new type of solitary waves in a one-dimensional granular medium. *Journal of Applied Mechanics and Technical Physics*, 26(3):405–408, 1985.

[32] E. Hascoët and H. J. Herrmann. Shocks in non-loaded bead chains with impurities. *The European Physical Journal B - Condensed Matter and Complex Systems*, 14(1):183–190, 2000.

[33] M. Manciu, S. Sen, and A. J. Hurd. Crossing of identical solitary waves in a chain of elastic beads. *Phys. Rev. E*, 63:016614, 2000.

[34] F. S. Manciu and S. Sen. Secondary solitary wave formation in systems with generalized hertz interactions. *Phys. Rev. E*, 66:016616, 2002.

[35] J. Hong and A. Xu. Nondestructive identification of impurities in granular medium. *Applied Physics Letters*, 81(25):4868–4870, 2002.

[36] V. F. Nesterenko, C. Daraio, E. B. Herbold, and S. Jin. Anomalous wave reflection at the interface of two strongly nonlinear granular media. *Phys. Rev. Lett.*, 95:158702, 2005.

[37] J. Hong. Universal power-law decay of the impulse energy in granular protectors. *Phys. Rev. Lett.*, 94:108001, 2005.

[38] R. Doney and S. Sen. Decorated, tapered, and highly nonlinear granular chain. *Phys. Rev. Lett.*, 97:155502, 2006.

[39] M. Manciu. *Nonlinear acoustics of granular media*. PhD thesis, SUNY-Buffalo, 2000.

[40] M. A. Porter, C. Daraio, E. B. Herbold, I. Szelengowicz, and P. G. Kevrekidis. Highly nonlinear solitary waves in periodic dimer granular chains. *Phys. Rev. E*, 77:015601, 2008.

[41] N. Boechler, G. Theocharis, S. Job, P. G. Kevrekidis, Mason A. Porter, and C. Daraio. Discrete breathers in one-dimensional diatomic granular crystals. *Phys. Rev. Lett.*, 104:244302, 2010.

[42] G. Theocharis, N. Boechler, P. G. Kevrekidis, S. Job, Mason A. Porter, and C. Daraio. Intrinsic energy localization through discrete gap breathers in one-dimensional diatomic granular crystals. *Phys. Rev. E*, 82:056604, 2010.

[43] URL `www.python.org`.

[44] URL `http://www.numpy.org`.

[45] URL `www.scipy.org`.

[46] scipy.integrate.ode, 2008. URL `http://docs.scipy.org/doc/scipy/reference/generated/scipy.integrate.ode.html`.

[47] P. N. Brown, G. D. Byrne, and A. C. Hindmarsh. Vode: A variable-coefficient ode solver. *SIAM Journal on Scientific and Statistical Computing*, 10(5):1038–1051, 1989.

[48] G. D. Byrne and A. C. Hindmarsh. A polyalgorithm for the numerical solution of ordinary differential equations. *ACM Trans. Math. Softw.*, 1(1):71–96, 1975.

[49] P. N. Brown and A. C. Hindmarsh. Vode source code. URL `http://www.netlib.org/ode/vode.f`.

[50] V. F. Nesterenko. Solitary waves in discrete media with anomalous compressibility and similar to "sonic vacuum". *Journal de Physique IV Colloque*, 04(C8): 729–734, 1994.

[51] V. F. Nesterenko. Pulse compression nature in a strongly nonlinear grained medium. *Proc. of the International Symposium on Intense Dynamic Loading and its Effects*, pages 236–239, 1992.

[52] E. J. Hinch and S. Saint–Jean. The fragmentation of a line of balls by an impact. *Proceedings of the Royal Society of London A: Mathematical, Physical and Engineering Sciences*, 455(1989):3201–3220, 1999.

[53] C. Daraio, V. F. Nesterenko, E. B. Herbold, and S. Jin. Energy trapping and shock disintegration in a composite granular medium. *Phys. Rev. Lett.*, 96: 058002, 2006.

[54] D. Leng, X. Wang, G. Liu, and L. Sun. Impulse absorption by horizontal magnetic granular chain. *AIP Advances*, 6(2):025321, 2016.

[55] A. M. Tichler, L. R. Gómez, N. Upadhyaya, X. Campman, V. F. Nesterenko, and V. Vitelli. Transmission and reflection of strongly nonlinear solitary waves at granular interfaces. *Phys. Rev. Lett.*, 111:048001, 2013.

Repository references

[A] C3MassInterfaceSmallLarge.mp4
[B] C3MassInterfaceLargeSmall.mp4
[C] C3GranularContainer.mp4
[D] oneDim.py
[E] C5WavePropagationSmallExponent.mp4
[F] C5WavePropagationLargeExponent.mp4
[G] C6IncreasingExponentInterface.mp4
[H] C6DecreasingExponentInterface.mp4
[I] C6IncreasingExponentImpurity.mp4
[J] C6DecreasingExponentImpurity.mp4
[K] C7Disorder.mp4
[L] C7PeriodicityCollective.mp4
[M] C7PeriodicityDecay.mp4
[N] C7PeriodicityPeriodicWaveform.mp4